NASA TECHNICAL NOTE

NASA TN D-5030

EXPLORATORY INVESTIGATION OF
FLOW FIELD RESULTING FROM
FORWARD-FACING NOZZLES EXHAUSTING
NEAR A LARGE CYLINDRICAL BODY AT
FREE-STREAM MACH NUMBERS OF 3.0 AND 6.0

by Robert J. McGhee and James A. Martin

Langley Research Center
Langley Station, Hampton, Va.

EXPLORATORY INVESTIGATION OF

FLOW FIELD RESULTING FROM FORWARD-FACING NOZZLES

EXHAUSTING NEAR A LARGE CYLINDRICAL BODY AT

FREE-STREAM MACH NUMBERS OF 3.0 AND 6.0

By Robert J. McGhee and James A. Martin

Langley Research Center
Langley Station, Hampton, Va.

Page Intentionally Left Blank

EXPLORATORY INVESTIGATION OF
FLOW FIELD RESULTING FROM FORWARD-FACING NOZZLES
EXHAUSTING NEAR A LARGE CYLINDRICAL BODY AT
FREE-STREAM MACH NUMBERS OF 3.0 AND 6.0

By Robert J. McGhee and James A. Martin
Langley Research Center

SUMMARY

Some effects of forward-facing supersonic conical nozzles exhausting into an oncoming stream near a large cylindrical body have been investigated for free-stream Mach numbers of 3.0 and 6.0 and for angles of attack of 0° to 4°. Schlieren data and surface pressure data in the vicinity of one of the nozzles on the body were obtained for nozzle-exhaust Mach numbers of 2.20 and 3.68. For a jet-exit Mach number of 2.20, the range of jet-exit to free-stream static-pressure ratio was from 0 (jet off) to about 2800 at a free-stream Mach number of 6.0 and from 0 to about 400 for a free-stream Mach number of 3.0. The Reynolds number per meter was approximately 6.89×10^6 and 3.61×10^6 at free-stream Mach numbers of 3.0 and 6.0, respectively.

The investigation showed that the resulting flow field contained extensive regions of boundary-layer separation and mixing adjacent to the cylindrical body. The extent of flow separation on the body depended upon the ratio of jet-exit static pressure to free-stream static pressure, jet-exit Mach number, and free-stream Mach number. An extensive wake region, caused by the limited expansion of the jet exhaust flow at the nozzle lip, was observed around the nozzles and body base at all test conditions. Increasing the angle of attack from 0° to 4° had only a minor effect on the flow field. Large local surface pressures resulted from the initial impingement of the nozzle exhaust on the body. The pressure coefficient on the body just forward of the nozzle exit, when based on jet-exit conditions, was independent of the ratio of jet-exit static pressure to free-stream static pressure and free-stream Mach number.

INTRODUCTION

During flight of rocket vehicles at high altitudes and high Mach numbers, the rocket-motor nozzles often exhaust at pressures far greater than the pressure of the surrounding environment. For even moderate underexpansion, large billowing exhaust plumes result

which may cause extensive boundary-layer separation, high surface heating, and large local loads, particularly if the jet exhaust impinges upon adjacent surfaces. Investigations of several such problems have been reported in references 1 to 3.

The present investigation was initiated to obtain information on the flow field which results when forward-facing supersonic nozzles are exhausted near a body into an oncoming hypersonic stream. This type of flow field results during staging of multiple-stage launch vehicles, where retrorockets are employed. Retrorockets are usually high-thrust, short-duration, solid-propellant engines arranged symmetrically around the launch vehicle and provide enough total impulse to achieve rapid separation of the stages. The influence on the flow field of the gases discharged by such engines is important from stability and control considerations. Also, solid-propellant exhaust gases are highly ionized and can interrupt vehicle-to-ground communications during staging, an important factor from the mission-control viewpoint.

This report presents preliminary results obtained by injecting gaseous nitrogen from conical supersonic nozzles into an oncoming stream at Mach numbers of 3.0 and 6.0. The basic model consisted of a circular cylinder approximately 8 diameters long with a conical forebody.

The investigation was conducted in a 2-foot hypersonic facility at the Langley Research Center. The Reynolds number per meter was approximately 6.89×10^6 and 3.61×10^6 at free-stream Mach numbers of 3.0 and 6.0, respectively. The angle of attack was varied from 0° to 4°.

SYMBOLS

$C_{p,4}$ impingement pressure coefficient, $\dfrac{p_4 - p_j}{q_j}$

$\left(C_{p,4}\right)_{Mod}$ modified pressure coefficient, $\dfrac{\dfrac{p_4}{p_\infty} - \dfrac{p_j}{p_\infty}}{\dfrac{\gamma_j}{2} M_j{}^2 \dfrac{\left(T/T_t\right)_j}{\beta_j}}$

d diameter of cylinder, 6.71 cm

M_∞ free-stream Mach number

M_j jet-exit Mach number

p local surface static pressure

p_j jet-exit static pressure

p_4 static pressure at orifice 4 (see fig. 2)

p_∞ free-stream static pressure

q_j jet dynamic pressure

$\left(T/T_t\right)_j$ ratio of static temperature to stagnation temperature of jet

x/d orifice location measured from model base in body diameters

α angle of attack, deg

ϕ angular location of orifices 5 and 6, deg (see fig. 2)

$\beta_j = \sqrt{M_j^2 - 1}$

γ_j ratio of specific heats of jet

APPARATUS AND TESTS

Model

A sketch of the general arrangement of the model is shown in figure 1 and model details are shown in figure 2. The 16° half-angle conical forebody and circular cylinder were constructed of aluminum except for the rear section of the cylinder. This section was constructed of steel and housed the plenum chamber for the compressed gas supply to four simulated nozzles. The compressed gas passed through a hollow sting and was admitted into the plenum chamber through louvers.

The two conical nozzle configurations (fig. 2) used in the investigation provided exit Mach numbers of 2.20 and 3.68. Gaseous nitrogen at local atmospheric temperature was the exhaust medium. The nozzles, typical retronozzles for a representative large launch vehicle, were designed to simulate the plume shape with the aid of the techniques given in reference 4. The nozzles were fabricated so they could be attached or removed from the nozzle holders. Caps were provided so that any combination of one to four nozzles could be tested.

Wind Tunnel

The tests were conducted in a 2-foot hypersonic facility at the Langley Research Center. This wind tunnel, described in reference 5, is an ejector type which provides continuous flow at high Mach numbers and low densities. The average test conditions are shown in the following table:

M	Stagnation temperature, ^{o}K	Stagnation pressure, kN/m^2	Static pressure, kN/m^2	Reynolds number per m
3.0	311	101	2.34	6.89×10^6
6.0	422	319	.2	3.61×10^6

Nitrogen Supply

High-pressure gaseous nitrogen was generated by pumping liquid nitrogen to the required storage pressure and converting it from liquid to gas in a steam-actuated heat exchanger. The high-pressure gaseous nitrogen was then stored in a tank farm with a capacity of 22.65 m^3. Suitable pressure-reducing and pressure-regulating valves were remotely controlled to obtain the nitrogen gas pressure in a manifold outside the test section which in turn fed the nozzle plenum chamber in the model. Once the correct pressure was obtained in the manifold, a quick-acting guillotine valve was employed to initiate and terminate the flow to the nozzles. Minor pressure adjustments could be made after initiation of flow through the nozzles.

Instrumentation

Six static pressure orifices (0.15 cm in diameter) were located on the body surface, four in the plane of symmetry forward of the top-mounted nozzle, and two laterally displaced as shown in figure 2. Simultaneous measurements of the six orifice pressures, as well as the nozzle plenum pressure, were obtained from absolute pressure measuring transducers. Data were obtained by a high-speed data acquisition system and recorded on magnetic tape. In addition, schlieren photographs taken at each datum point with the use of a 2-microsecond flash from a xenon light source were used for a visual study of the jet interaction phenomena.

Tests and Accuracy

The model was tested with the M_j = 2.20 and 3.68 nozzles at free-stream Mach numbers of 3.0 and 6.0. With the M_j = 2.20 nozzle, p_j/p_∞ varied from 0 (jet off) to about 2740 at M = 6.0 and from 0 to 386 at M = 3.0. When the M_j = 3.68 nozzle was used, p_j/p_∞ varied from 0 to about 553 at M = 6.0 and from 0 to 37 at M = 3.0. The model angle of attack was adjusted to obtain data at 0°, 2°, and 4°. All data were obtained

4

with the model smooth; that is, no boundary-layer transition strips were used. At the Reynolds numbers of these tests, laminar flow was considered to exist over almost the entire model except for some test conditions at $M = 3.0$, where the flow was probably transitional over the rear of the model.

The ratios of p_j/p_∞ quoted herein are estimated to be accurate within ± 2 percent. The Mach number in the region of the test model was accurate within ± 0.04. Angle-of-attack values are estimated to be accurate within $\pm 0.2^O$. Because of the complex flow field resulting from jet interaction with the free stream, the absolute level of accuracy of the local static pressures is difficult to establish. The static-pressure ratios varied from about $p/p_\infty = 1$ to about $p/p_\infty = 150$ for the orifice closest to the nozzle exit. Figure 3 indicates the repeatability of the data taken during different test runs. The values of p/p_∞ presented should be interpreted as indicative primarily of the general trends and levels for a complex flow environment.

RESULTS AND DISCUSSION

The results of this investigation have been arranged to illustrate the flow field which results when forward-facing nozzles are exhausted near a body into an oncoming stream at $M = 3.0$ and 6.0. Figure 4 is a diagram of the simplified flow-field model illustrating several portions of the flow field of particular interest. These portions of the flow field can be observed in the representative schlieren photographs and corresponding pressure data in figures 5 to 7, which illustrate the effects on the flow field of jet-pressure ratio, angle of attack, and number of nozzles firing. Complete surface pressure data for all configurations tested are presented in figures 8 to 14, and a correlation of impingement pressures is shown in figures 15 to 17.

Flow-Field Model

A simplified model of the flow field has been devised from the schlieren photographs and is illustrated in figure 4. The flow field shown is for a free-stream Mach number of 6.0, a low jet-pressure ratio, all four nozzles firing, and an angle of attack of 0°; however, the features indicated are representative of those for other Mach numbers and jet-pressure ratios. There are four portions of the flow field: the primary flow (initially the free stream), the secondary flow (originating as the exhaust flow from the nozzles and turning outward and rearward), a viscosity-induced portion (bounded by the primary and secondary flows and the body), and the wake (behind the body and secondary flow).

Primary flow.- The primary flow, which is initially the undisturbed free stream, is first compressed by a conical bow shock wave and a conical flow field over the forebody.

5

An expansion occurs at the shoulder and turns the flow field along the body surface and also weakens the bow shock wave. A compression shock wave is then required near the point of boundary-layer separation to turn the flow outward along the dividing streamline between the primary flow and the viscosity-induced portion of the flow field. Another shock wave, originating at the initial juncture of the primary and secondary flows, turns the primary flow still farther outward. The flow direction is then parallel to the dividing streamline between the primary and secondary flows. The primary flow, for conditions similar to those of this model, remains entirely supersonic.

The primary flow field is similar to the corresponding portion of the flow field of a cone-cylinder-flare. The last shock wave corresponds to the shock wave originating at the reattachment point on the flare.

Secondary flow.- The secondary flow originates as the exhaust flow from the nozzles. It issues supersonically from the nozzles and expands three dimensionally at the nozzle lip to the local pressure of the wake. Although the wake pressure is much less than the jet-exit static pressure, the turning angle of the nozzle flow is limited to that for expansion to infinite Mach number. For the jet-exit Mach numbers of this investigation, this limiting turning angle was less than 100°, and the schlieren photographs indicate that the total divergence of the nozzle flow did not exceed 90° (15° initial nozzle divergence and 75° turning angle) because of the finite pressure in the wake.

Along the inboard portion of the jet boundary, the exhaust flow impinges on the body and is turned forward and parallel to the body surface. The resulting compression forms a shock wave which is visible in many of the schlieren photographs. This impinging part of the flow then separates from the body surface and turns upward away from the body. A shock wave is formed at the juncture of the primary and secondary flows, and the entire secondary flow is finally turned downstream parallel to the primary flow. At least one strong shock wave, in the form of a Mach disk, can be expected in the interior of the secondary flow, but only a few schlieren pictures show disturbances which could be interpreted as Mach disks.

Viscosity-induced portion.- The viscosity-induced portion of the flow field is bounded by the primary flow, the secondary flow, and the body. This portion of the flow consists of a separated region and a mixing region. The separated region has two zones of circulation: a forward zone of clockwise flow and a rearward zone of counterclockwise flow. The mixing region is the result of the initial interaction of the primary and secondary flows and is also the confluence of the viscous shear layers accompanying the dividing streamlines between the primary and secondary flows and the separated region.

Wake.- The wake is directly behind the body and nozzles and the rear boundaries of the secondary flow from the nozzles. The extreme size of the wake is the result of

6

the limited expansion of the secondary flow at the nozzle lip, which causes a large radial disturbance and separates the primary flow from the wake by the secondary flow.

Effect of Jet-Pressure Ratio

The investigation covered a wide range of jet-pressure ratios. The schlieren photographs in figures 5, 6, and 7 indicate that increasing the jet-pressure ratio increased the length along the body and the height above the body of the viscosity-induced portion of the flow field until the separation point of the primary flow approached the cone-cylinder juncture. The high pressure in the primary flow on the conical forebody retarded further forward movement of the separation streamline, and an additional increase in jet-pressure ratio primarily increased the angle of the separation streamline. (See fig. 5.) This increase in the angle of the separation streamline reduced the expansion angle at the cone-cylinder juncture, and the bow shock wave was weakened less than for the lower jet-pressure ratios. The bow shock wave appeared to move outward from the body as a result of this increase in jet-pressure ratio. Further increases in jet-pressure ratio would probably move the separation point forward of the cone-cylinder juncture and detach the bow shock wave. However, it is not clear what phenomena would occur at jet-pressure ratios higher than those of the present investigation but lower than that required to detach the bow wave.

In addition to being a function of jet-pressure ratio, the extent of the viscosity-induced portion of the flow field is shown to be a function also of jet-exit Mach number and free-stream Mach number. For example, the higher jet-pressure ratios at $M_\infty = 3.0$ overlap the lowest jet-pressure ratio at $M_\infty = 6.0$, but the flow fields are quite different. (Compare figs. 5(a) concluded and 5(b).) Because of the exploratory nature of this investigation, the relationships of the characteristics of the flow field to these parameters have not been determined.

Effect of Angle of Attack

Figure 5(c) shows the resulting flow field for 2^O and 4° angle of attack at $M_\infty = 6.0$. A comparison of figure 5(c) with figure 5(b) ($\alpha = 0^O$) indicates that the positive angles of attack increased the angle of the separation streamline above the body (and decreased it below the body) by approximately 10 percent or less. The total displacement of the external flow, however, was not noticeably changed by these angles of attack. For $M_\infty = 3.0$ at positive angles of attack, no schlieren photographs were available with all four nozzles firing, but the pressure distributions in figures 8 and 13 show the same aerodynamic trends as the data for $M_\infty = 6.0$.

Effect of Number of Nozzles

The results discussed thus far are for all four nozzles firing simultaneously. The effect of a single nozzle firing can be seen in figures 6 and 7; data are presented for the $M_j = 2.20$ nozzle at both $M_\infty = 3.0$ and $M_\infty = 6.0$ and for the $M_j = 3.68$ nozzle at $M_\infty = 3.0$. On the side of the body with the nozzle firing, the secondary flow remains much closer to the body than when all four nozzles are firing. On the opposite side of the body, the circumferential spreading of the flow separation can be observed. For all but the lowest jet-pressure ratios of the investigation, some separation occurred completely around the body. For the higher jet-pressure ratios at $M_\infty = 6.0$, the point of boundary-layer separation approached the cone-cylinder juncture completely around the body. These observations indicate that considerable mutual interference exists between the secondary flows of the nozzles when multiple nozzles are operating at the jet-pressure ratios of this investigation.

Surface Pressure Distributions

The measured surface pressures of various nozzle arrangements are presented as functions of x/d in figures 8 to 12 for $\alpha = 0^O$, 2^O, and 4° and as functions of p_j/p_∞ in figures 13 and 14 for $\alpha = 0^O$. These data show that a wide range of local surface pressure will result from the operation of forward-facing nozzles on a vehicle. For example, the pressure orifice nearest the nozzle-exit plane measured values of p/p_∞ from about 1 at jet-off conditions to about 150 at $p_j/p_\infty = 2600$. At the most forward orifice locations, the measured pressure variations are small compared with the initial impingement pressure near the nozzle exit. Large local surface loads and high surface heating would be expected from the type of impingement shown in the data from this investigation.

Correlation of Impingement Pressure Data

Considerable attention has been given to the proper choice of a combination of the independent parameters to correlate the flow-field characteristics resulting from the injection of a supersonic secondary flow into a supersonic or hypersonic primary flow. For example, reference 6 indicated that for two-dimensional nozzles exhausting from a flat plate, jet mass flow was the important correlating parameter.

Figures 13 and 14 indicate that p_4/p_∞ varies approximately linearly with p_j/p_∞ for the present investigation, and this linear variation suggests the possibility of correlating the impingement pressure with jet-exit pressure ratio. If a pressure coefficient is formed so that

$$C_{p,4} = \frac{p_4 - p_j}{q_j} = \frac{\dfrac{p_4}{p_\infty} - \dfrac{p_j}{p_\infty}}{\dfrac{\gamma_j}{2} M_j{}^2 \dfrac{p_j}{p_\infty}} \tag{1}$$

then

$$\frac{p_4}{p_\infty} = \left(1 + \frac{\gamma_j}{2} M_j{}^2 C_{p,4}\right) \frac{p_j}{p_\infty} \tag{2}$$

For a given jet Mach number, $C_{p,4}$ is not a function of p_j/p_∞ since p_4/p_∞ varies linearly with p_j/p_∞, and the extended line passes through or near the origin. This is shown to be valid in figure 15.

Figure 15 also indicates that $C_{p,4}$ is not a function of free-stream Mach number. Since the data for $M_\infty = 3.0$ and $M_\infty = 6.0$ coincide, only one parameter in this investigation controlled $C_{p,4}$, that is, the jet-exit Mach number. Figure 16 represents an attempt to determine the dependence of $C_{p,4}$ on jet-exit Mach number. For convenience, the data and the functions have been normalized by their own values at $M_j = 2.20$. The curve for the common function

$$\frac{C_{p,4}}{\left(C_{p,4}\right)_{M_j=2.20}} = \frac{\left(\beta_j\right)_{M_j=2.20}}{\beta_j} \tag{3}$$

where $\beta_j = \sqrt{M_j{}^2 - 1}$, is shown by the figure not to be within the accuracy of the data. Further examination showed that the relation

$$C_{p,4} \propto \frac{\left(T/T_t\right)_j}{\beta_j} \tag{4}$$

where

$$\left(\frac{T}{T_t}\right)_j = \left(1 + \frac{\gamma_j - 1}{2} M_j{}^2\right)^{-1} \tag{5}$$

9

did agree with the data. If this is the correct dependence, then

$$\frac{\dfrac{p_4}{p_\infty} - \dfrac{p_j}{p_\infty}}{\dfrac{\gamma_j}{2} M_j^{\,2} \dfrac{(T/T_t)_j}{\beta_j}} \propto \frac{p_j}{p_\infty} \tag{6}$$

This modified pressure coefficient has been plotted in figure 17 and appears to correlate all the data from this investigation. The resulting relationship can be written as

$$\frac{p_4}{p_\infty} = \left[1 - 0.539\gamma_j M_j^{\,2} \frac{(T/T_t)_j}{\beta_j} \right] \frac{p_j}{p_\infty} \tag{7}$$

However, data were obtained for only two jet-exit Mach numbers, and no unique correlation can be definitely established without additional variations of this parameter.

The curves in figure 15 show that $C_{p,4}$ is not constant at the lower values of jet-exit-pressure ratio. Thus at these pressure ratios, orifice 4 is not in the proper location to measure the impingement pressure.

CONCLUDING REMARKS

Some of the effects of supersonic conical nozzles exhausting into an oncoming stream near a large cylindrical body have been investigated for free-stream Mach numbers of 3.0 and 6.0. The results suggest the following remarks:

1. The resulting flow field contained extensive regions of flow separation and mixing adjacent to the body. There was also an extensive wake around the nozzles which was due to the limited expansion at the nozzle lip.

2. The extent of flow separation depended upon jet static-pressure ratio, jet-exit Mach number, and free-stream Mach number.

3. Angle of attack had only a minor effect on the flow field.

4. Large local pressures resulted from the initial impingement of the nozzle exhaust on the body.

5. The pressure coefficient on the body surface just forward of the nozzle exit, when based on jet-exit conditions, was found to be independent of jet static-pressure ratio and free-stream Mach number.

Langley Research Center,
     National Aeronautics and Space Administration,
          Langley Station, Hampton, Va., December 2, 1968,
          126-13-03-39-23.

REFERENCES

1. McGhee, Robert J.: Some Effects of Jet Pluming on the Static Stability of Ballistic Bodies at a Mach Number of 6.00. NASA TN D-3698, 1966.

2. Hinson, William F.; and McGhee, Robert J.: Effects of Jet Pluming on the Static Stability of Five Rocket Models at Mach Numbers of 4, 5, and 6 and Static Pressure Ratios Up To 26 000. NASA TN D-4064, 1967.

3. Saturn V Engineering: Saturn V Exhaust Effects on Radio Systems Performance. Doc. No. D5-15606 (Contract NAS8-5608), Boeing Co., Oct. 3, 1966.

4. Pindzola, M.: Jet Simulation in Ground Test Facilities. AGARDograph 79, Nov. 1963.

5. Stokes, George M.: Description of a 2-Foot Hypersonic Facility at the Langley Research Center. NASA TN D-939, 1961.

6. Sterrett, James R.; Barber, John B.; Alston, Daisy W.; and Romeo, David J.: Experimental Investigation of Secondary Jets From Two-Dimensional Nozzles With Various Exit Mach Numbers For Hypersonic Control Application. NASA TN D-3795, 1967.

Forward-facing nozzles

16°

1.74 d

6.06 d

7.80 d

d
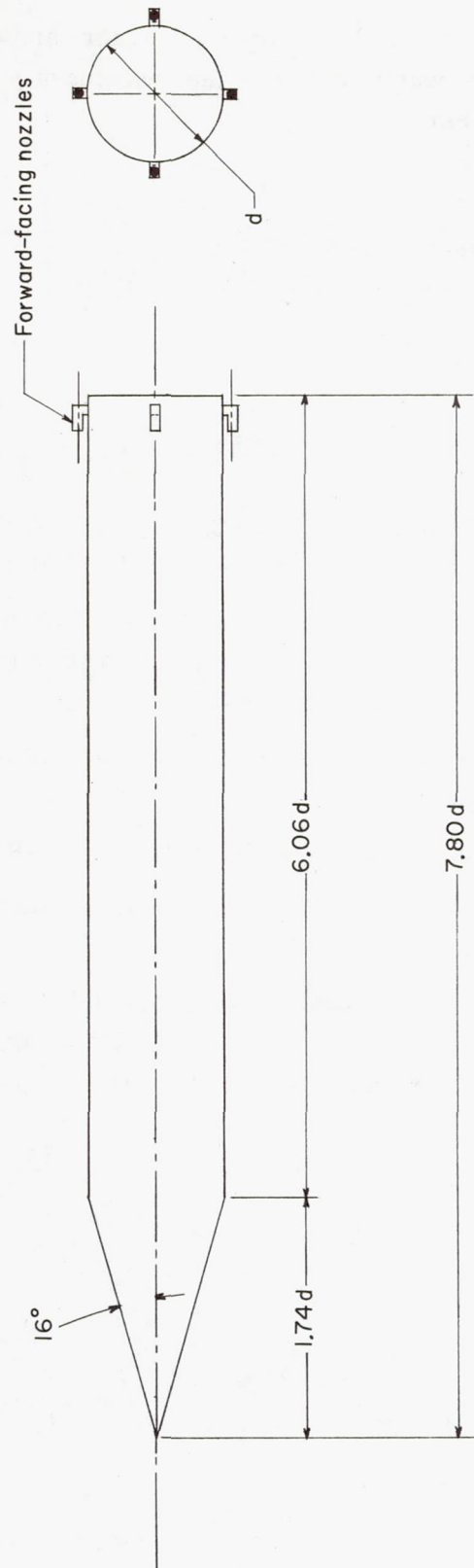
Figure 1.- General model arrangement. d = 6.71 cm.

12

Nozzle number →1

2 ○— —○ 4

3

Nozzle identification (rear view)

.076 d

.25 d

.19 d

.057 d

Nozzle center line

.19 d

From plenum chamber → ←Model base

←Model support sting

Nozzle location

x/d

1.52 d

1.14 d

.76 d

.38 d

φ

30°

45°

1 2 3 4
      5
      6

Orifice number

Orifice location
(top view)

Model base

.076 d
.046 d

15

.025 d

.0076 d

.081 d

.127 d

.0327 d

$M_j = 2.20$

←Nozzle flow

.076 d
.046 d

15

.056 d

.0076 d

.081 d

.127 d

.0164 d

$M_j = 3.68$
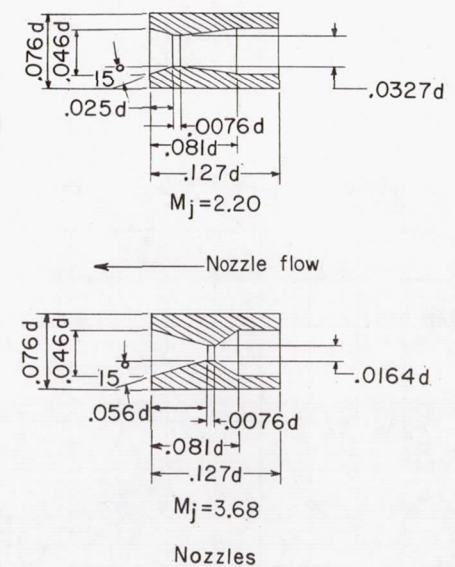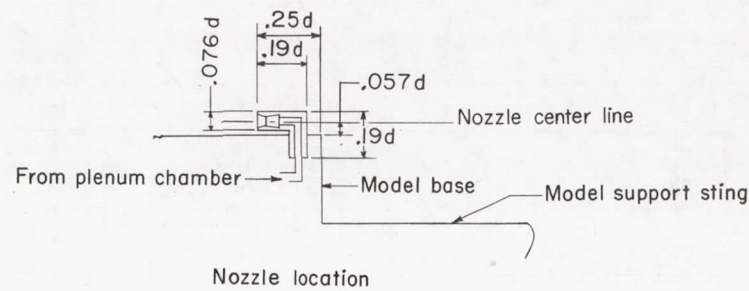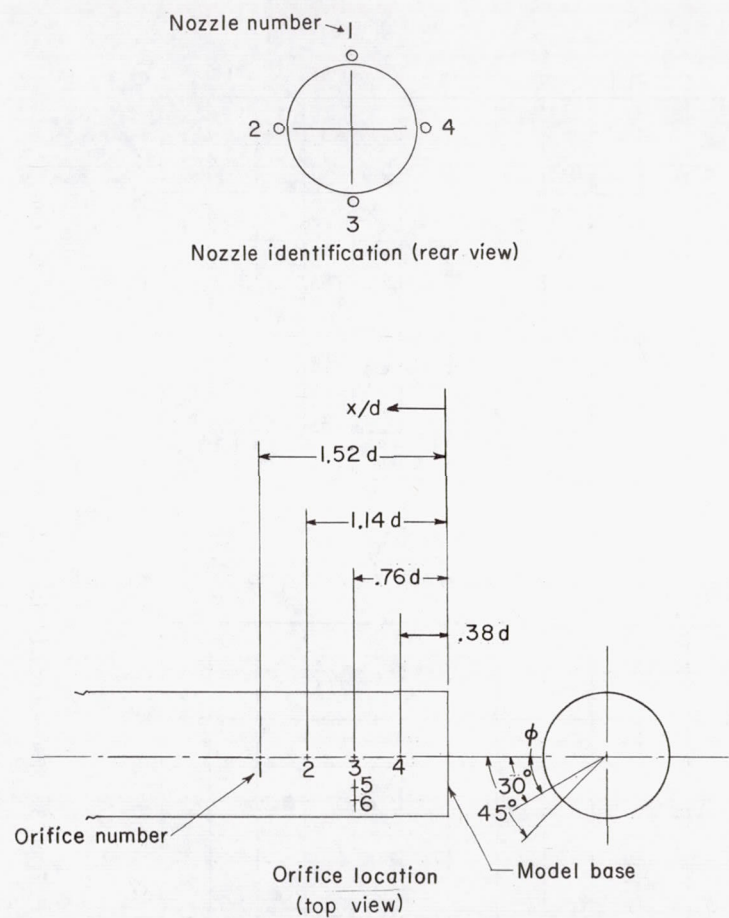
Nozzles

Figure 2.- Model details and orifice location. d = 6.71 cm.

13
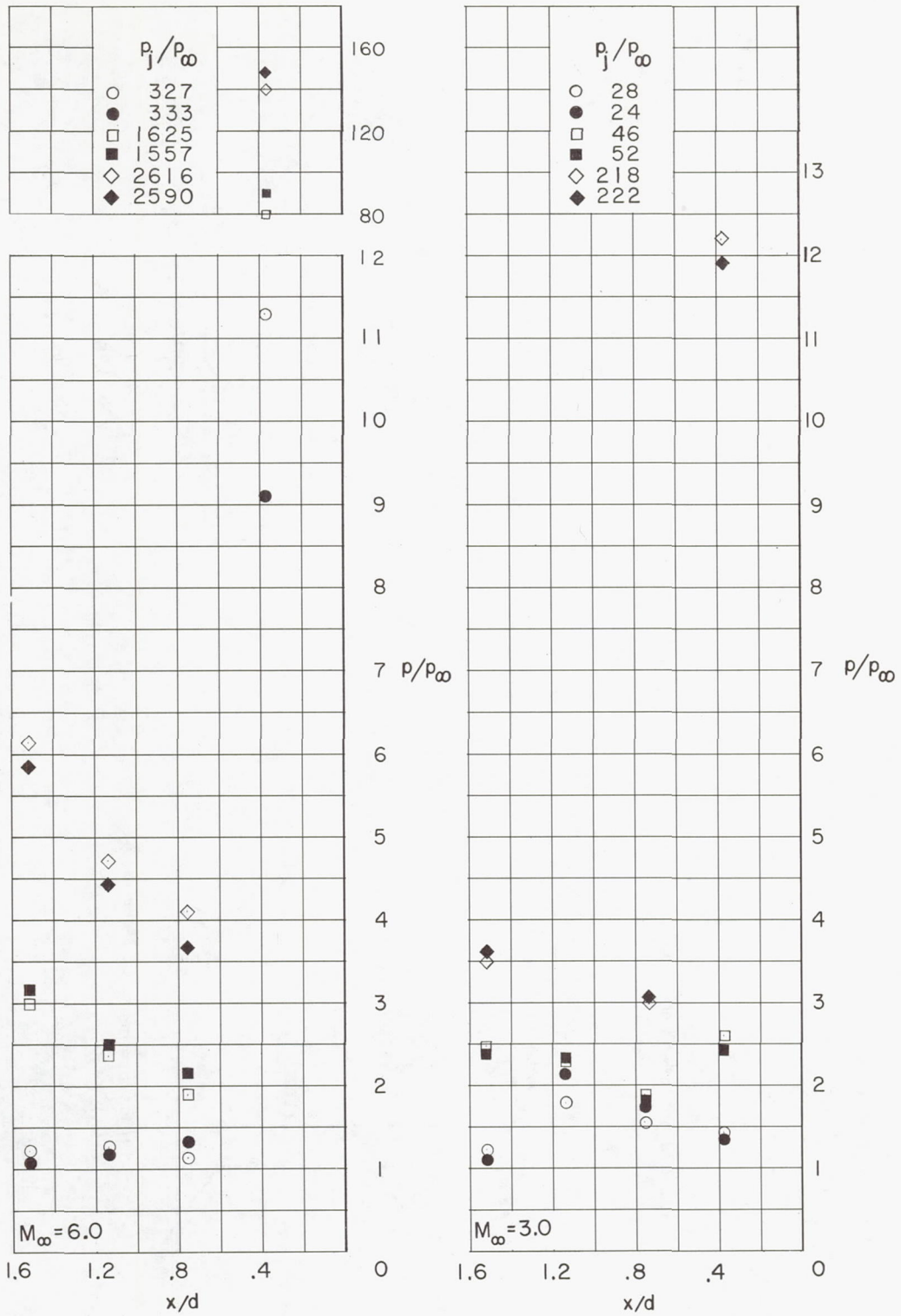
Figure 3.- Flow-field repeatability. $M_j = 2.20$; $\alpha = 0^0$; all four nozzles firing.
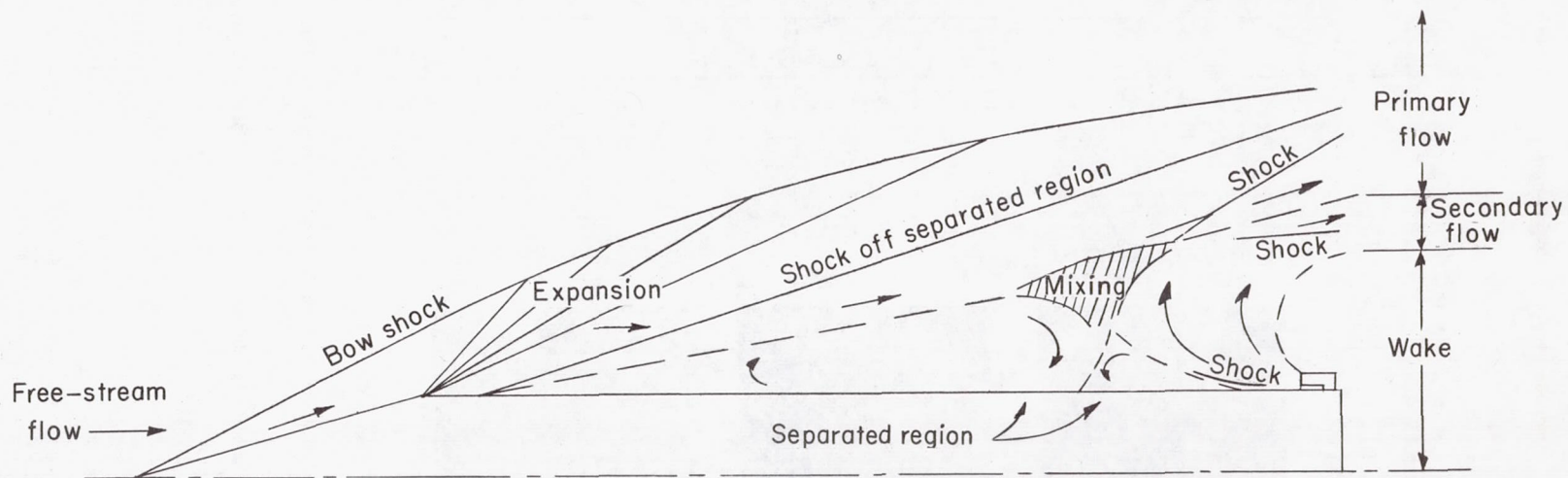
Figure 4.- Schematic representation of flow-field model.
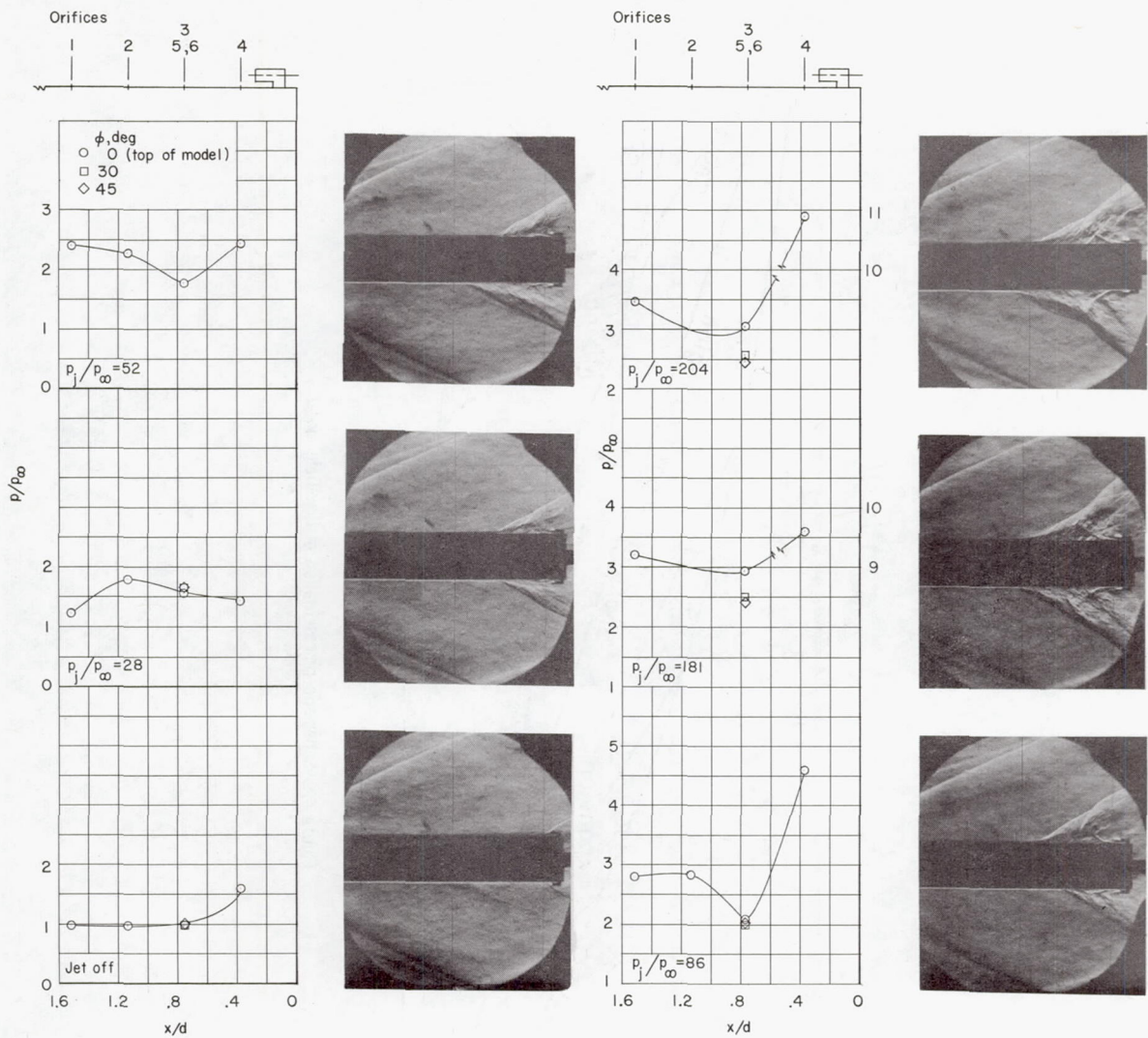
(a) $M_\infty = 3.0$; $\alpha = 0^0$. Points to the left of the break in the curve should be read from the left-hand scale; those to the right, from the right-hand scale.
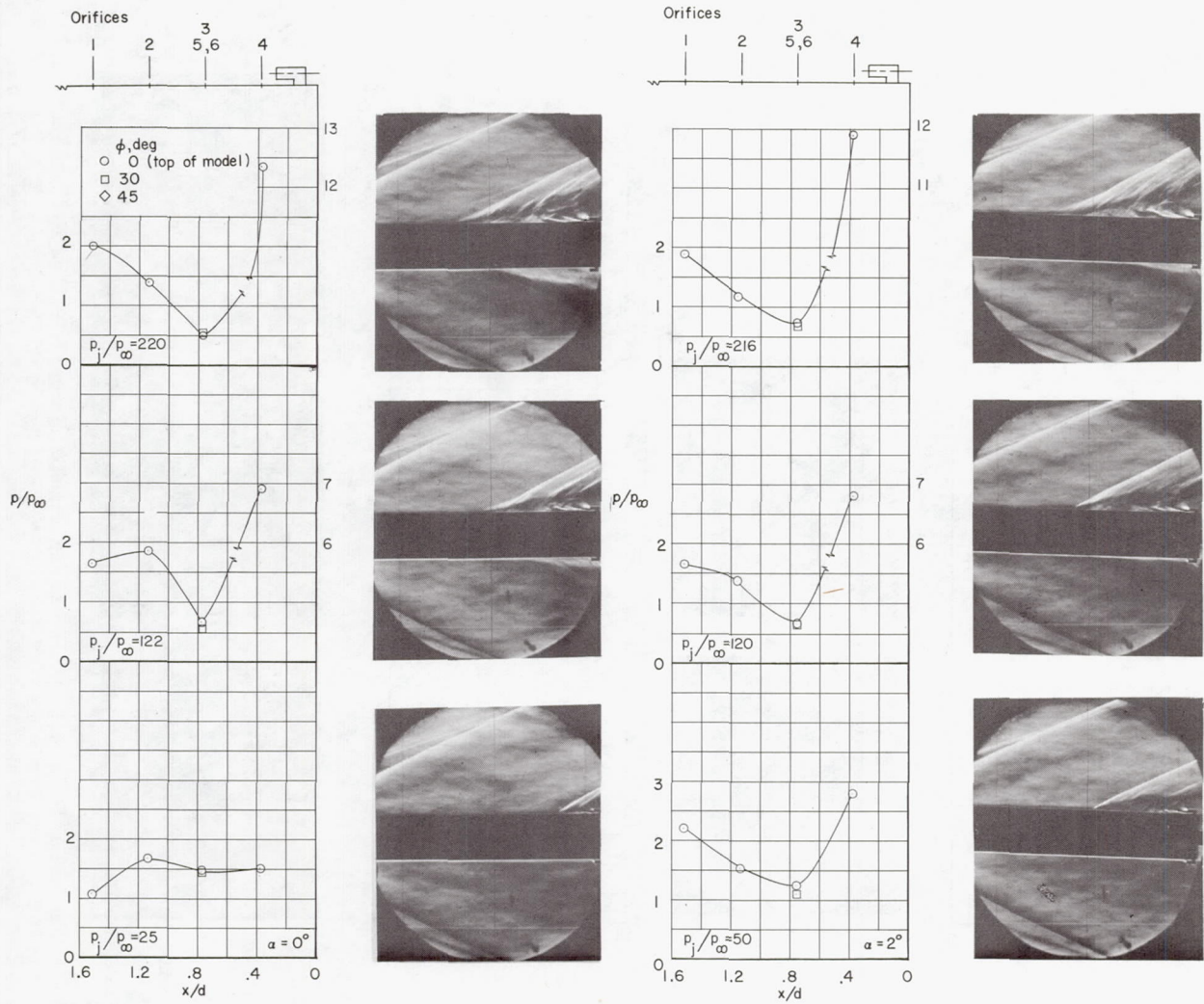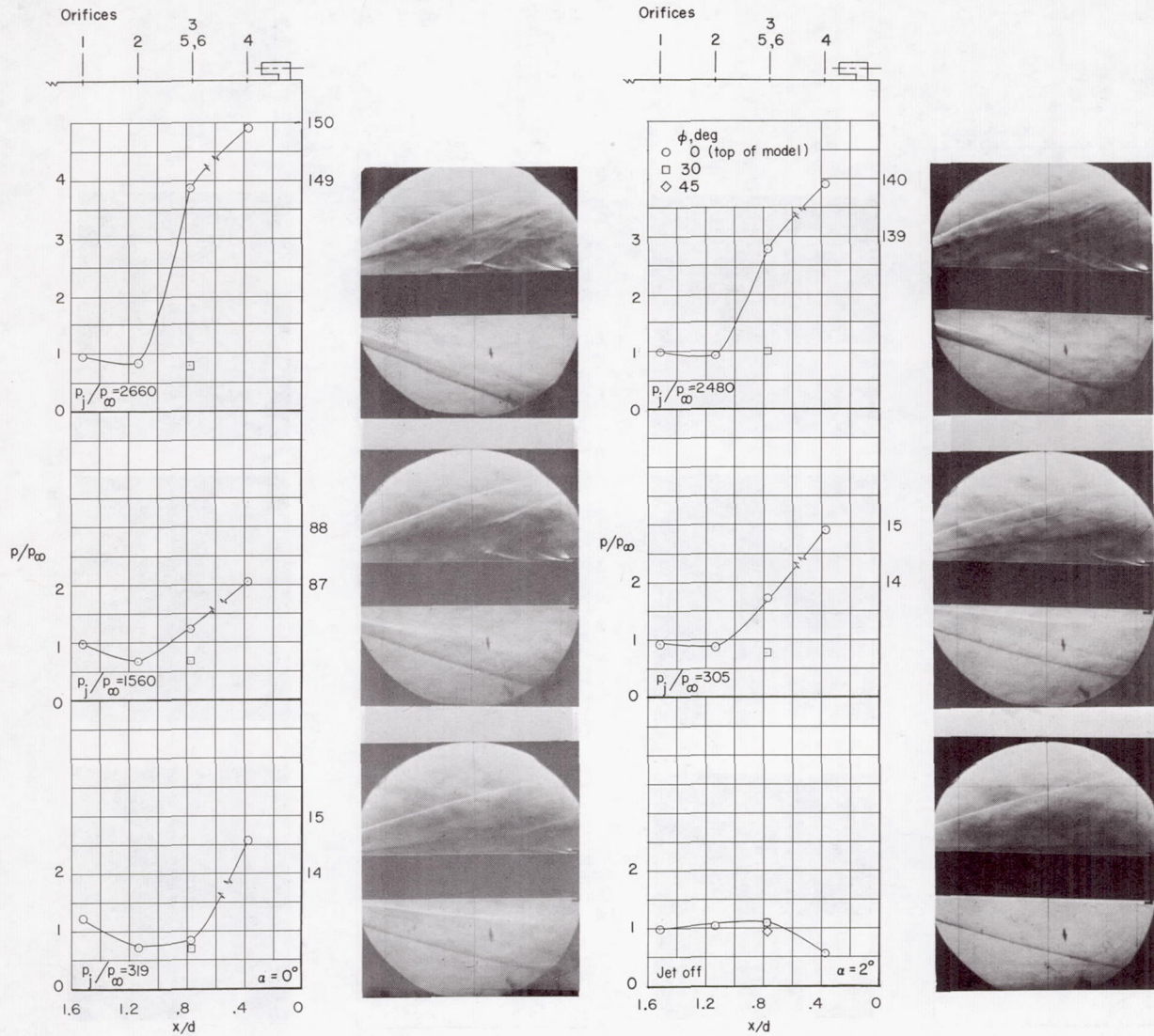
Figure 5.- Schlieren photographs and variation of p/p_∞ with x/d for $M_j = 2.20$. All four nozzles firing.

16
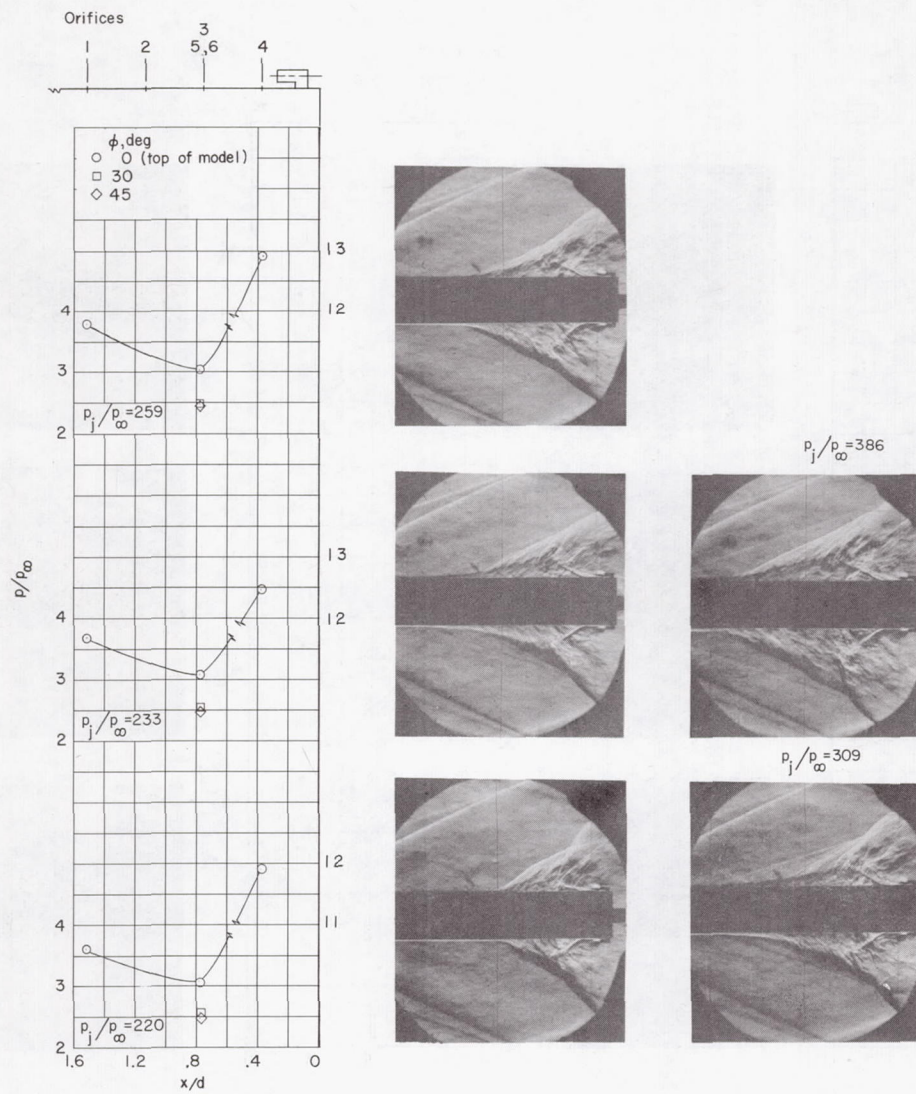
L-68-10,058

(a) Concluded. Points to the left of the break in the curve should be read from the left-hand scale; those to the right, from the right-hand scale.

Figure 5.- Continued.

Orifices

1 2 3 5,6 4

φ,deg
○ 0 (top of model)
□ 30
◇ 45

29
28

$p_j/p_\infty = 602$

p/p_∞

12
11

$p_j/p_\infty = 327$

3
2
1
Jet off

1.6   1.2   .8   .4   0
x/d

Orifices

1 2 3 5,6 4

6
5
4
3
$p_j/p_\infty = 2500$

135
134

p/p_∞

5
4
3
$p_j/p_\infty = 2150$

115
114

3
2
1
$p_j/p_\infty = 1557$

82
81

1.6   1.2   .8   .4   0
x/d

L-68-10,059

(b) $M_\infty = 6.0$; $\alpha = 0^0$. Points to the left of the break in the curve should be read from the left-hand scale; those to the right, from the right-hand scale.
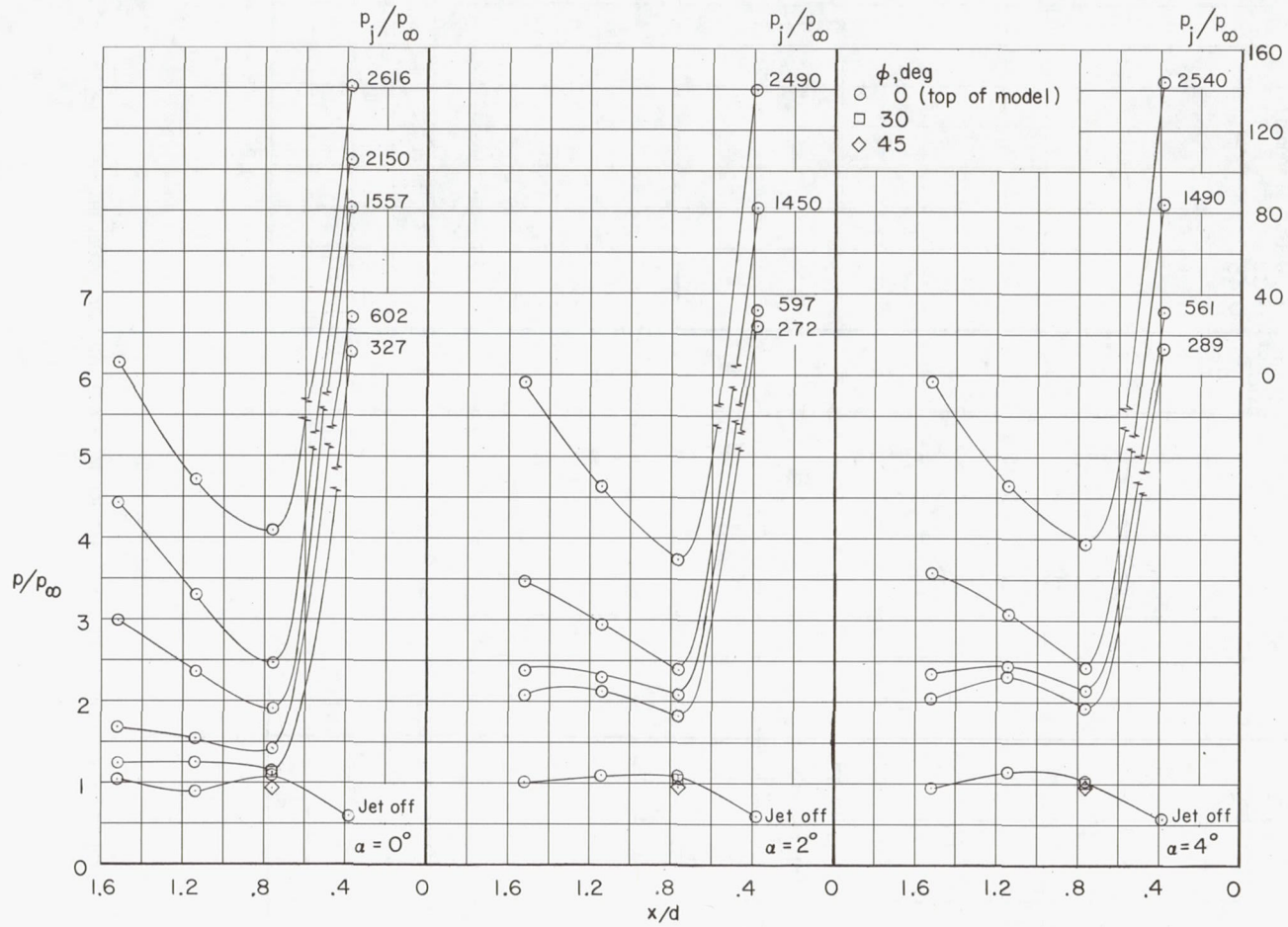
Figure 5.- Continued.

18
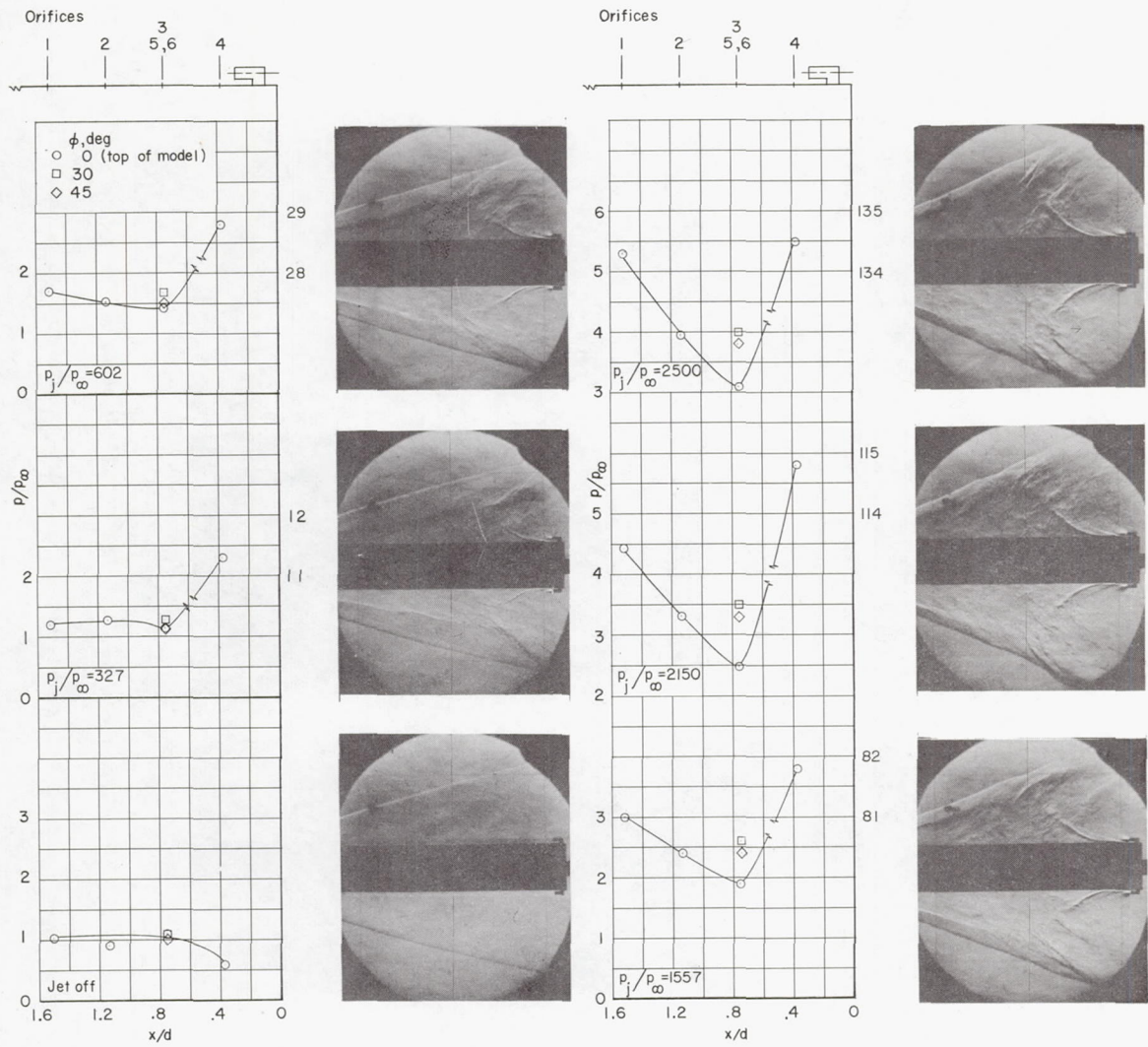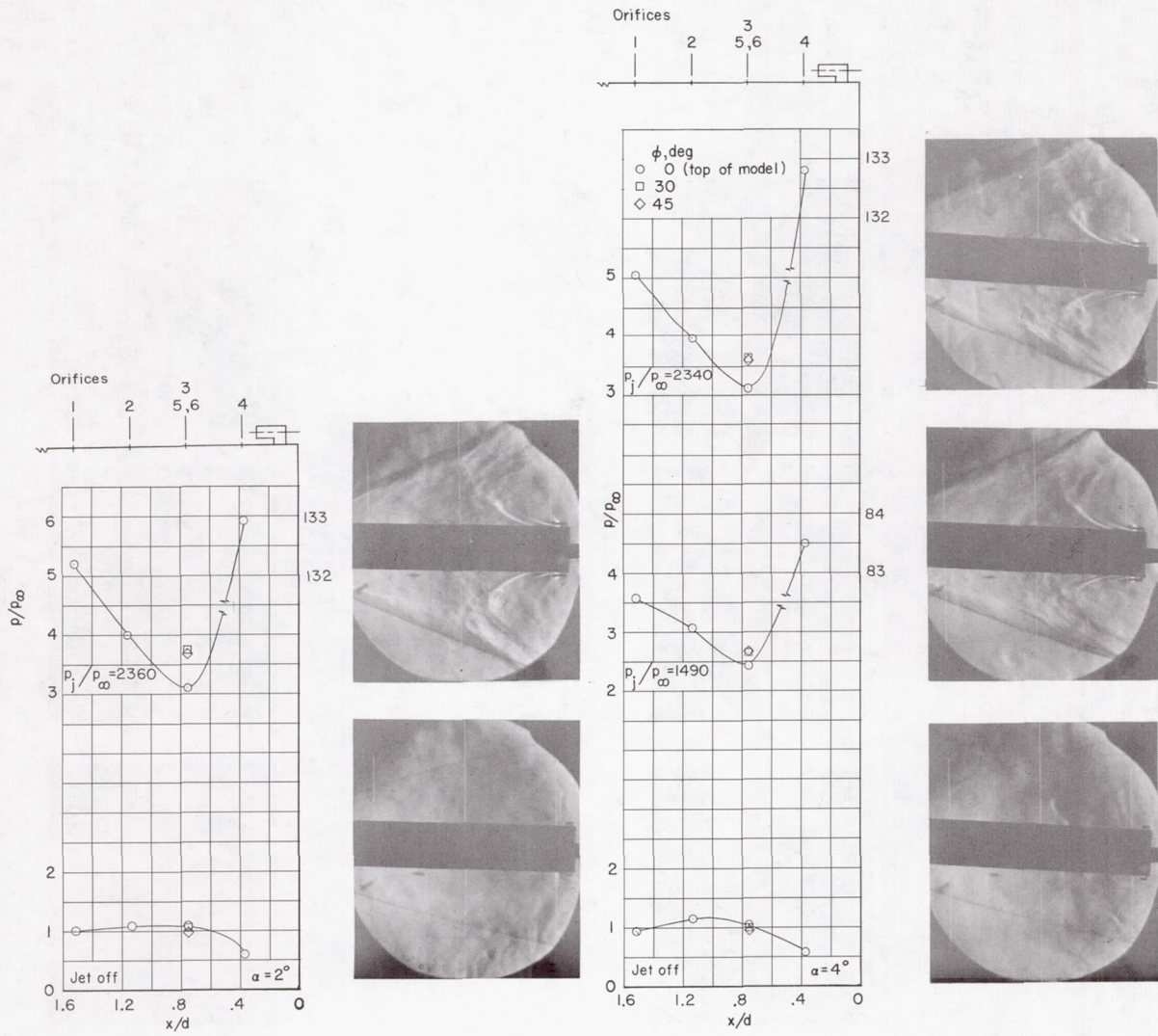
(c) $M_\infty = 6.0$; $\alpha = 2^0$ and 4^0. Points to the left of the break in the curve should be read from the left-hand scale; those to the right, from the right-hand scale.

Figure 5.- Concluded.

19

Orifices
1   2   3   4
    5,6

φ,deg
○ 0 (top of model)
□ 30
◇ 45

$p_j/p_\infty \approx 220$

p/p_∞

$p_j/p_\infty \approx 122$

$p_j/p_\infty \approx 25$ $\alpha = 0°$

1.6   1.2   .8   .4   0
x/d

Orifices
1   2   3   4
    5,6

$p_j/p_\infty \approx 216$

p/p_∞

$p_j/p_\infty \approx 120$

$p_j/p_\infty \approx 50$ $\alpha = 2°$

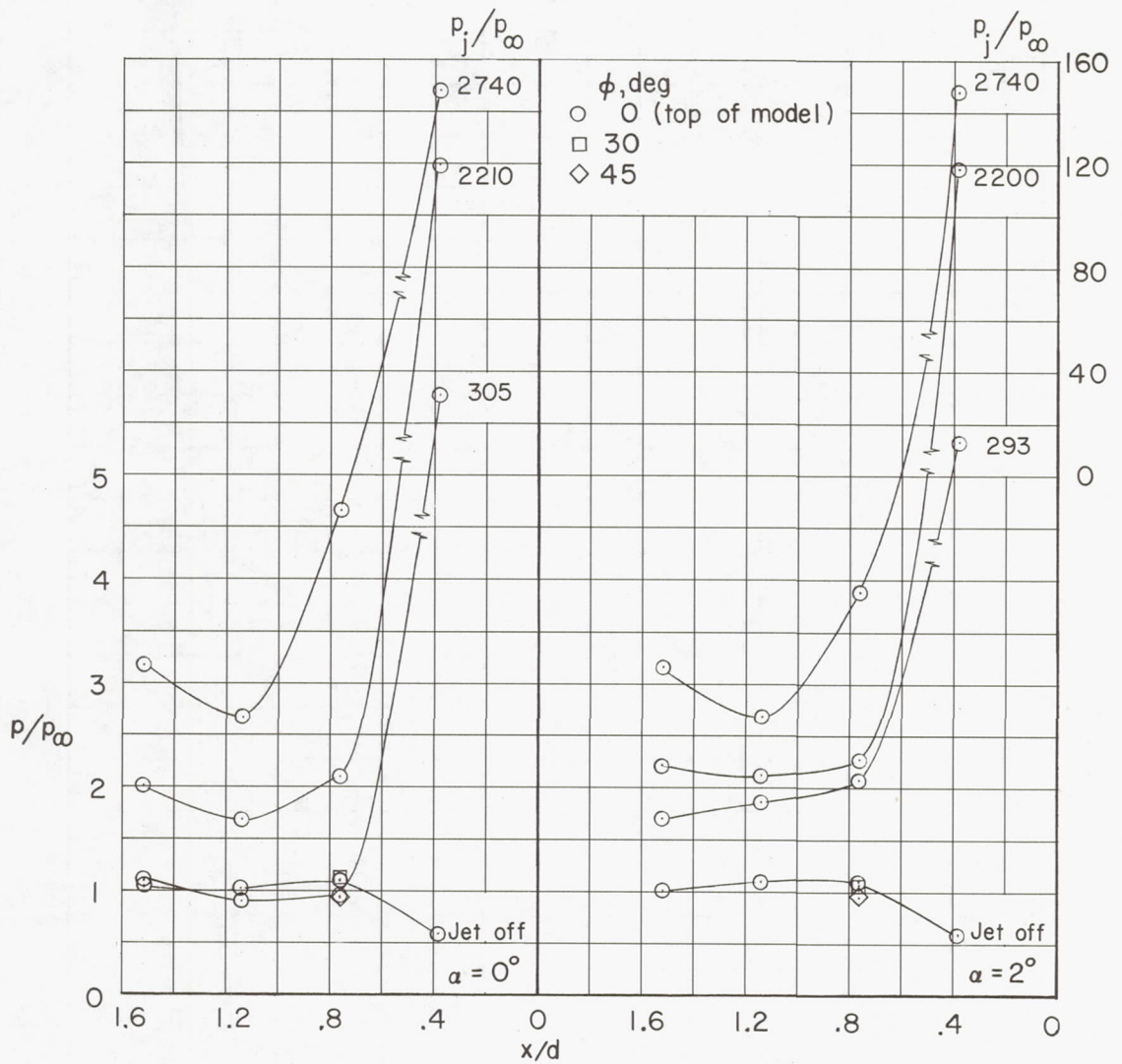1.6   1.2   .8   .4   0
x/d

L-68-10,061

(a) $M_\infty = 3.0$. Points to the left of the break in the curve should be read from the left-hand scale; those to the right, from the right-hand scale.

Figure 6.- Schlieren photographs and variation of p/p_∞ with x/d for $M_j = 2.20$. Nozzle 1 firing; $\alpha = 0°$ and $2°$.

Orifices

1   2   3   4
      5,6

p/p∞

150
149

$p_j/p_\infty = 2660$

88
87

$p_j/p_\infty = 1560$

15
14

$p_j/p_\infty = 319$ $\alpha = 0°$

1.6   1.2   .8   .4   0

x/d

Orifices

1   2   3   4
      5,6

φ, deg
○ 0 (top of model)
□ 30
◇ 45

140
139

$p_j/p_\infty = 2480$

15
14

$p_j/p_\infty = 305$

Jet off $\alpha = 2°$

1.6   1.2   .8   .4   0

x/d

L-68-10,062

(b) $M_\infty = 6.0$. Points to the left of the break in the curve should be read from the left-hand scale; those to the right, from the right-hand scale.
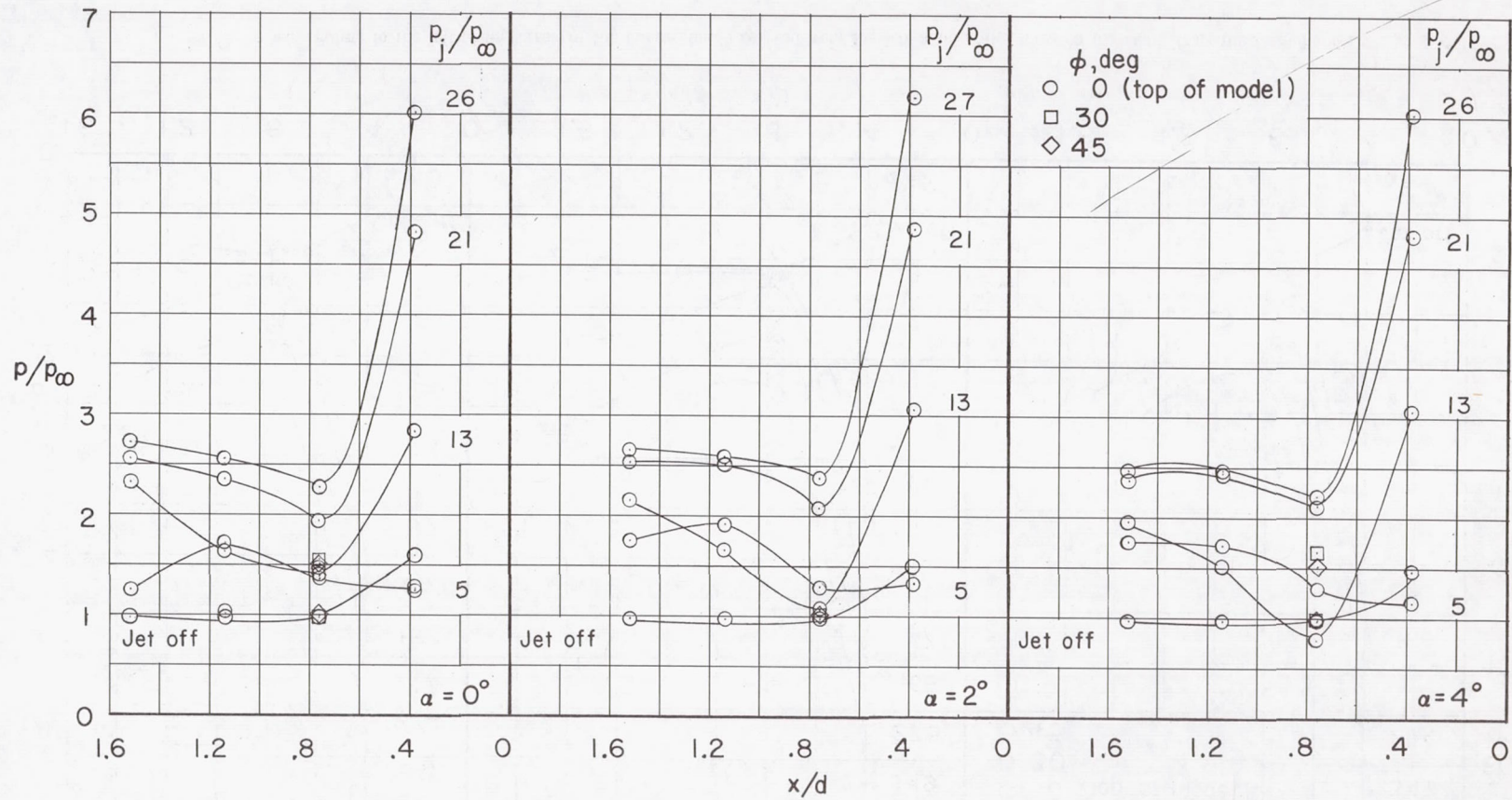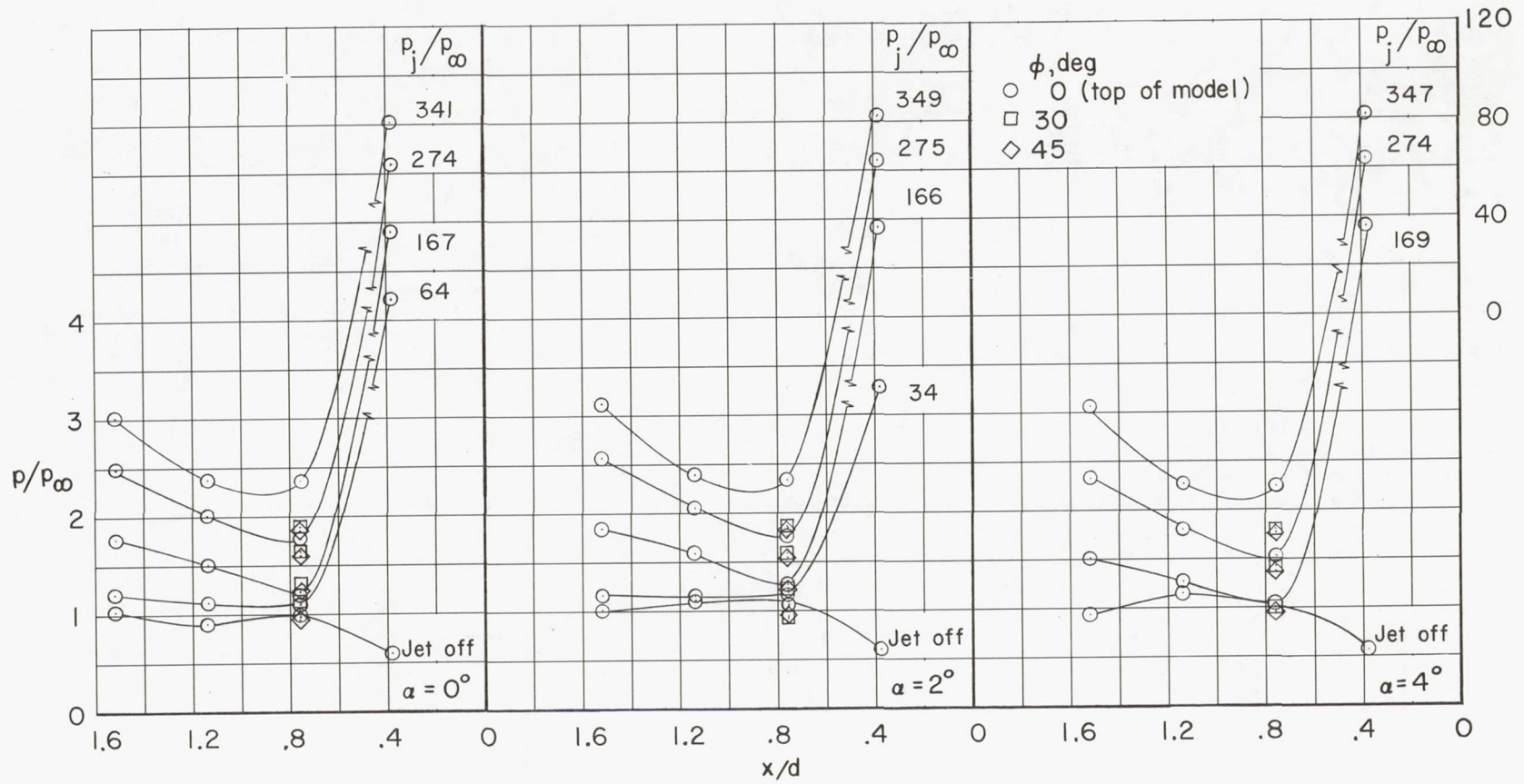
Figure 6.- Concluded.
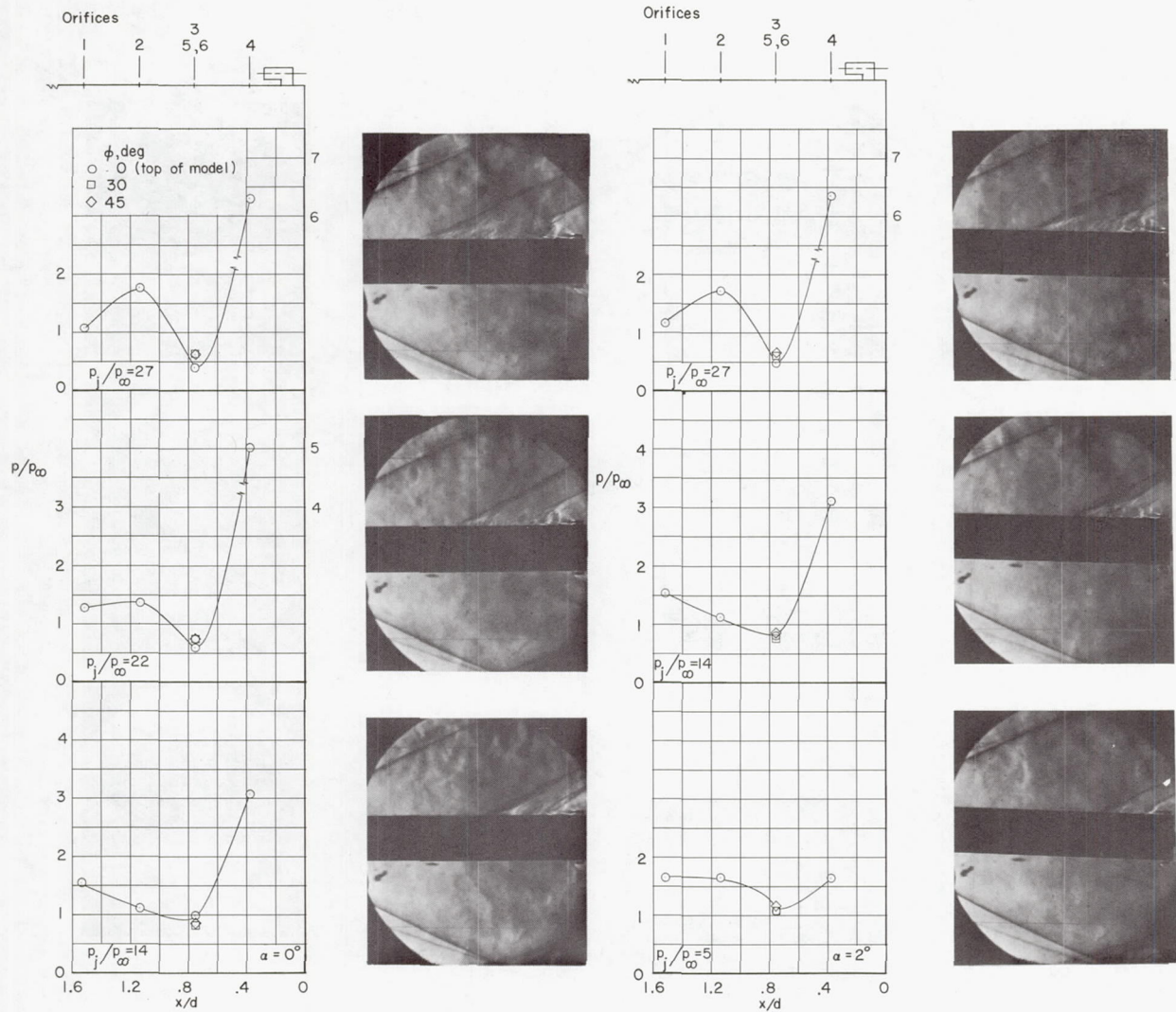
Figure 7.- Schlieren photographs and variation of p/p_∞ with x/d for $M_j = 3.68$. Nozzle 1 firing; $M_\infty = 3.0$. Points to the left of the break in the curve should be read from the left-hand scale; those to the right, from the right-hand scale.

L-68-10,063
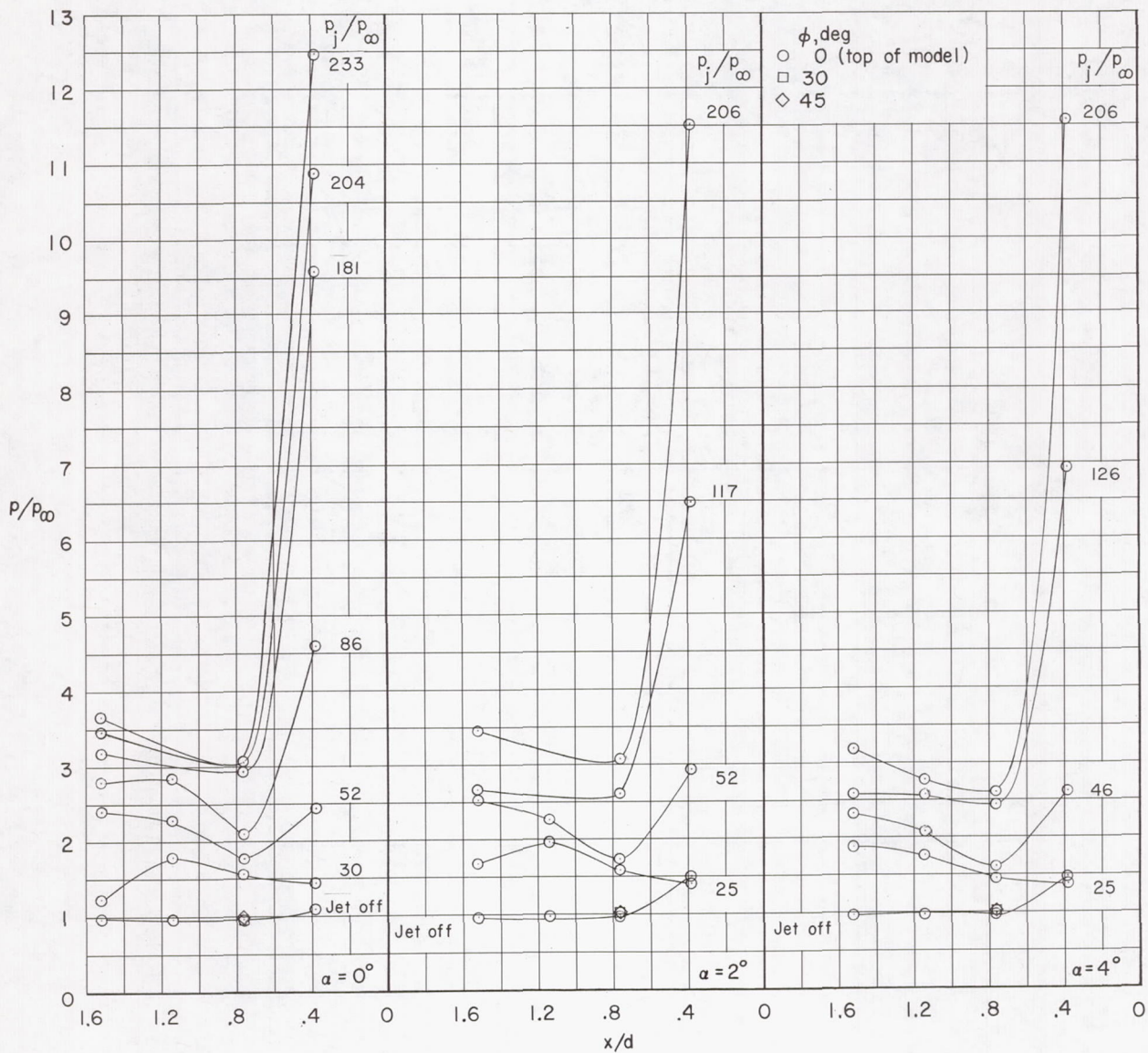
(a) $M_\infty = 3.0$.

Figure 8.- Variation of p/p_∞ with x/d for $M_j = 2.20$. All four nozzles firing.

(b) $M_\infty = 6.0$. Points to the left of the break in the curve should be read from the left-hand scale; those to the right, from the right-hand scale.
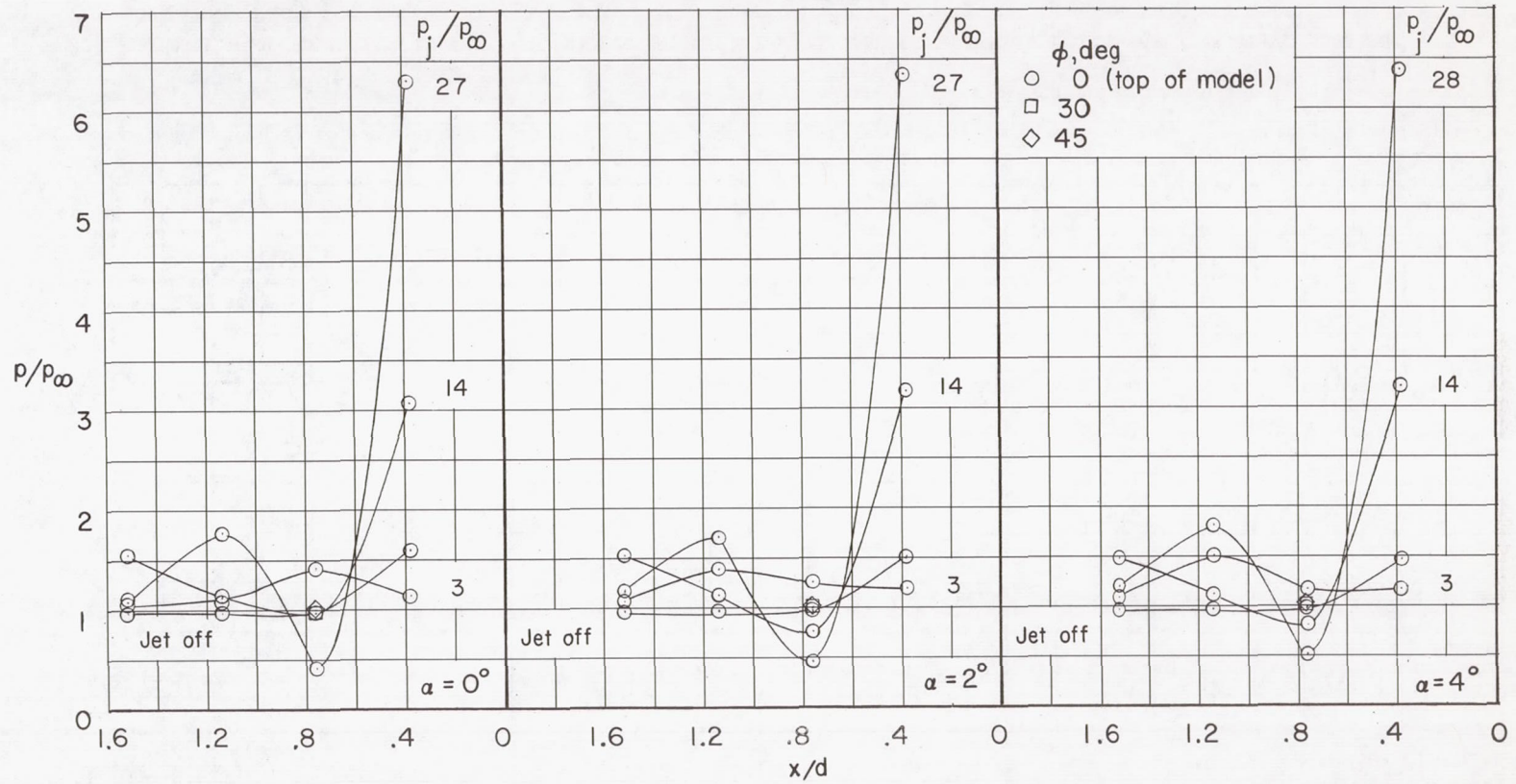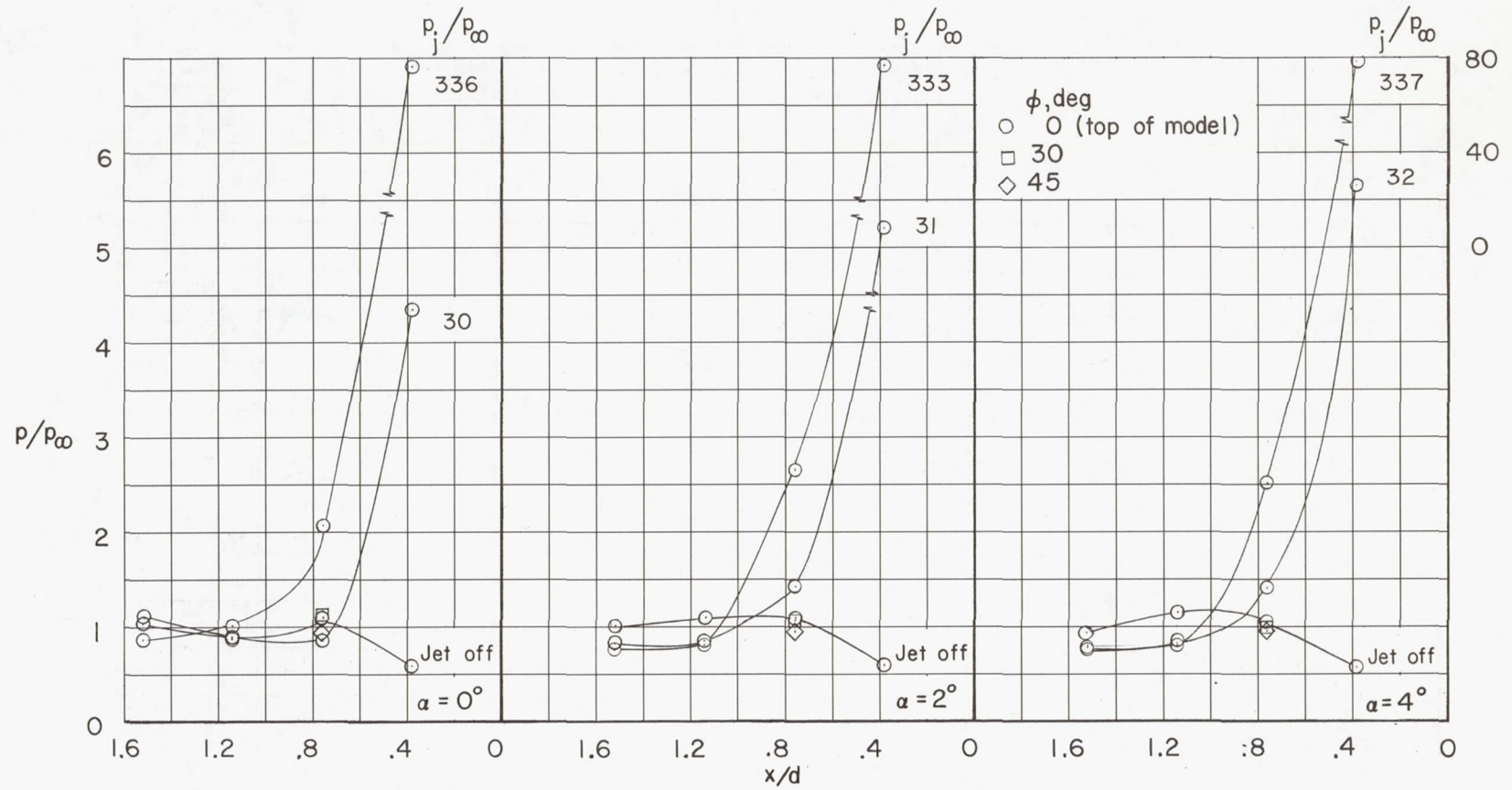
Figure 8.- Concluded.
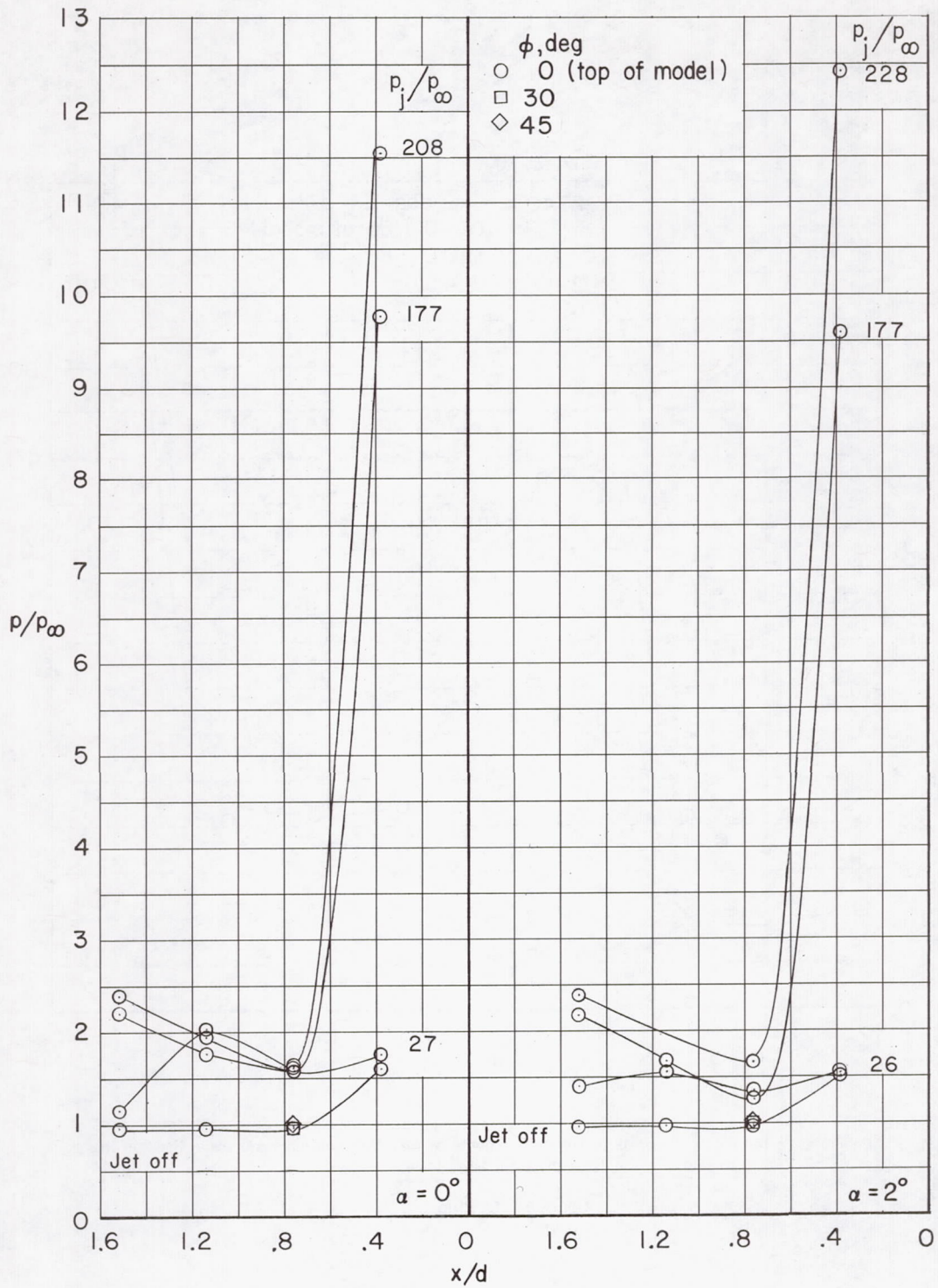
(a) $M_\infty = 3.0$.

Figure 9.- Variation of p/p_∞ with x/d for $M_j = 2.20$. Nozzles 1 and 3 firing.

(b) $M_\infty = 6.0$. Points to the left of the break in the curve should be read from the left-hand scale; those to the right, from the right-hand scale.
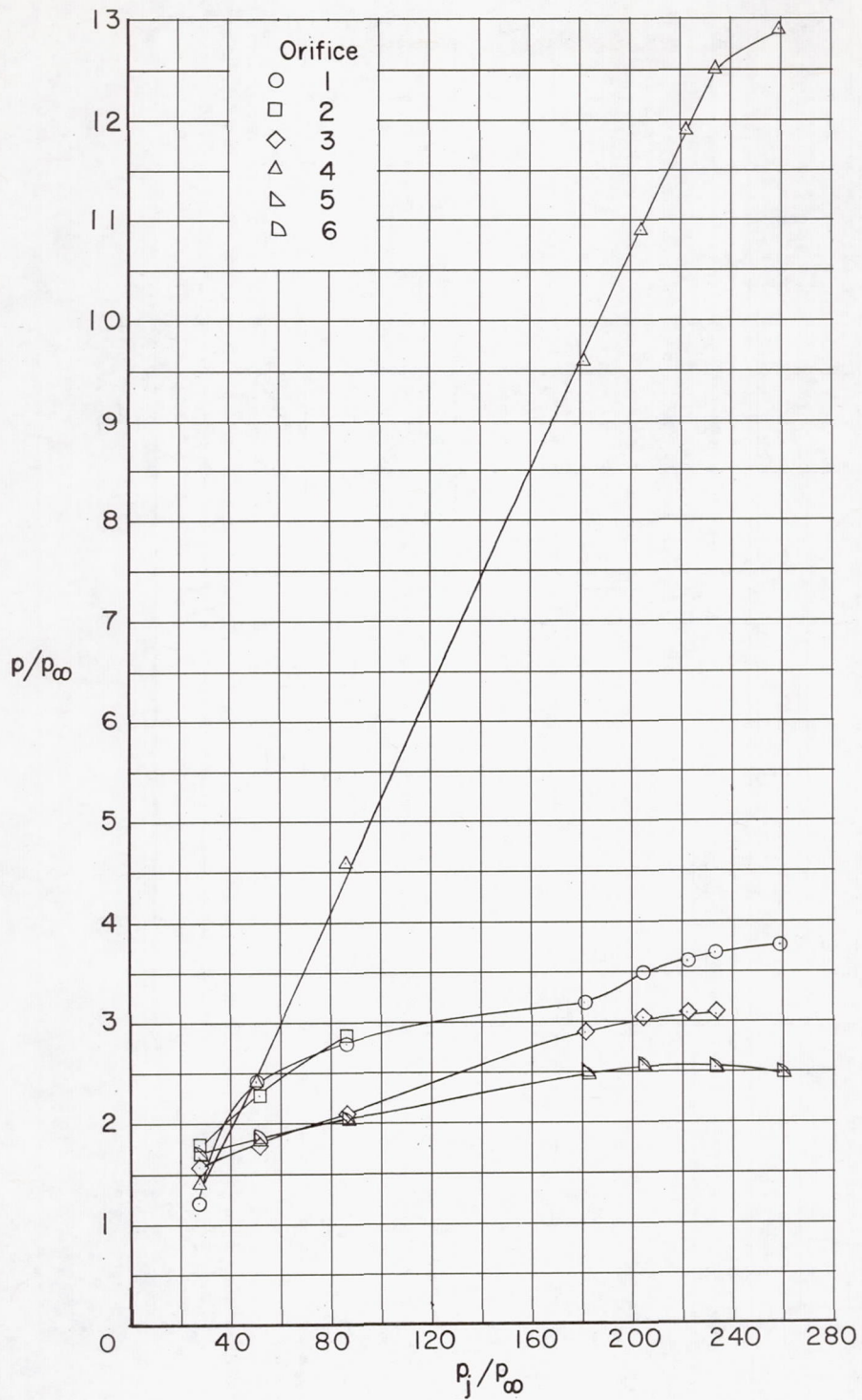
Figure 9.- Concluded.
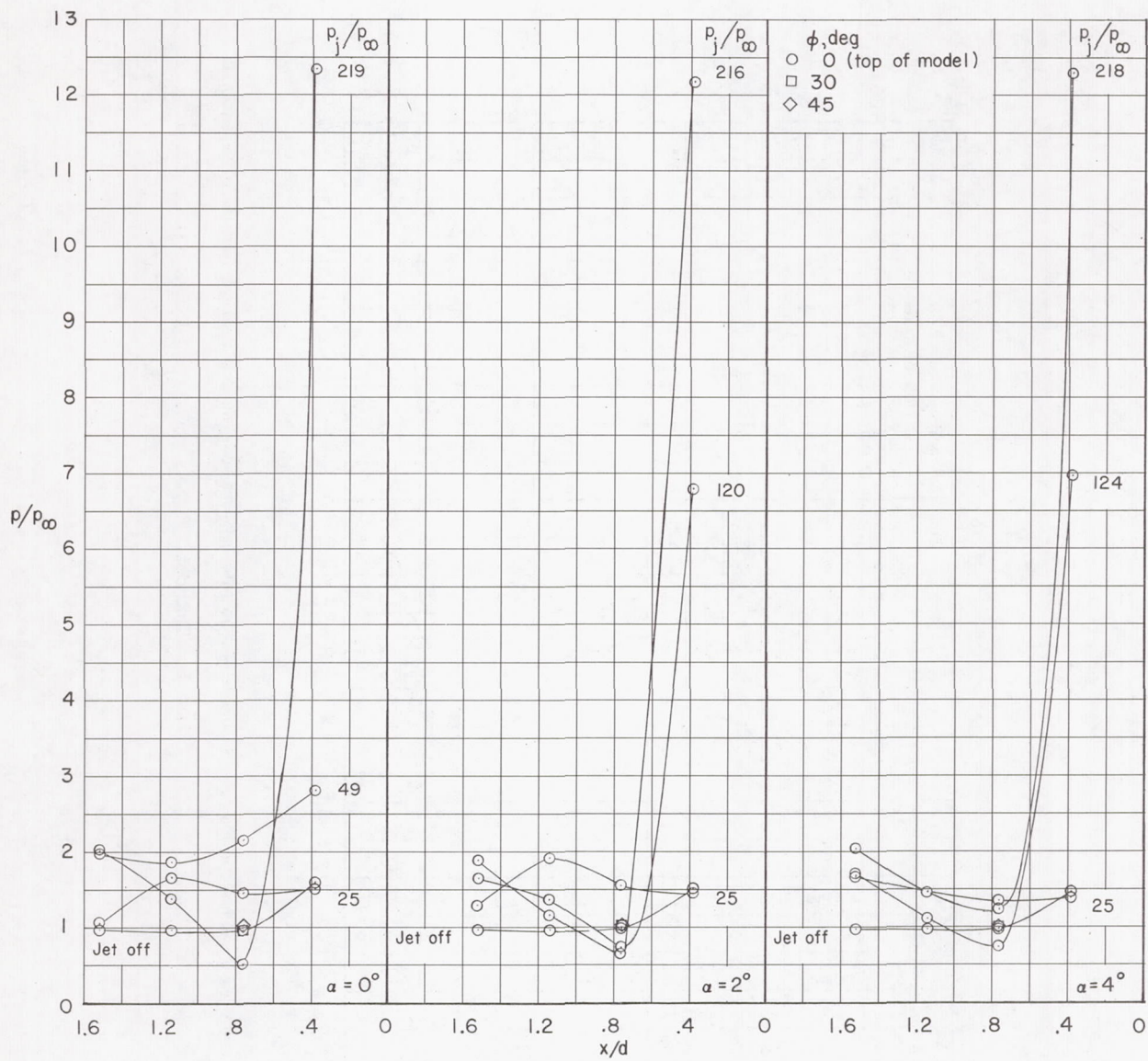
(a) $M_\infty = 3.0$.

Figure 10.- Variation of p/p_∞ with x/d for $M_j = 2.20$. Nozzle 1 firing.
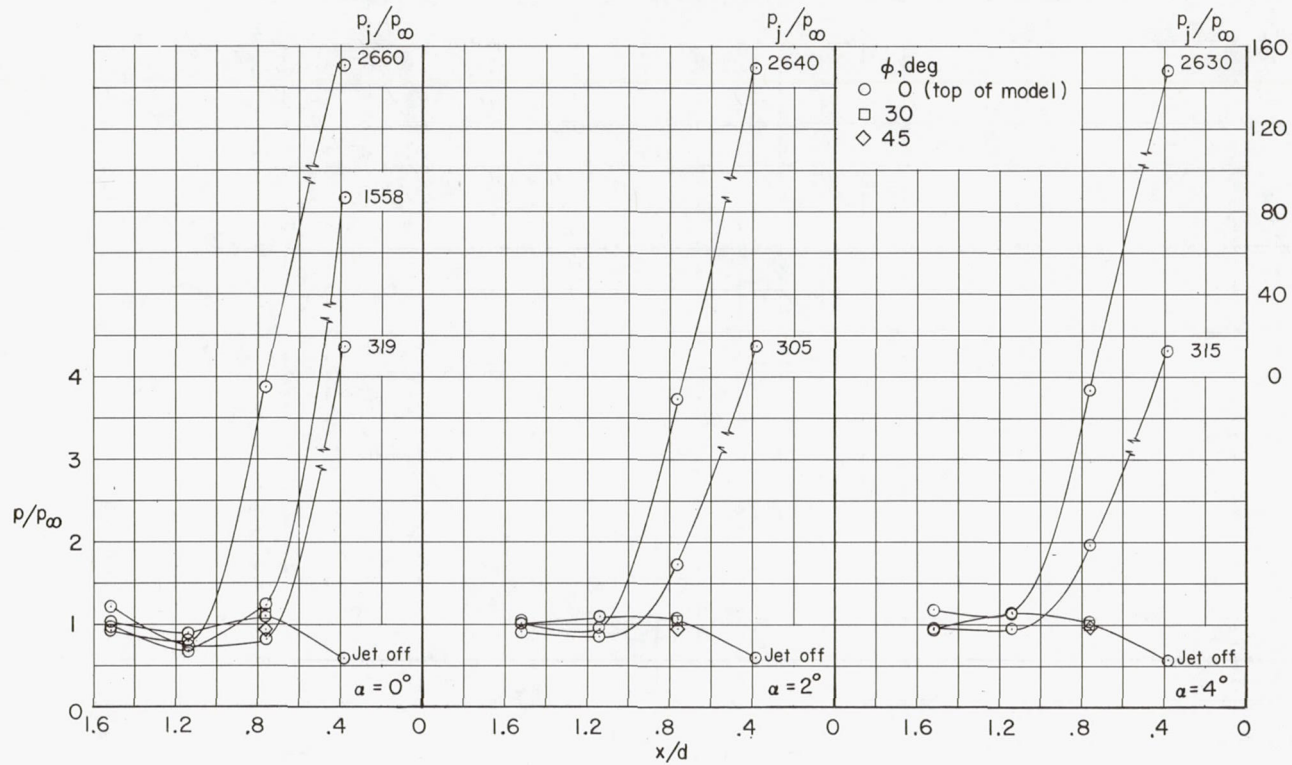
(b) $M_\infty = 6.0$. Points to the left of the break in the curve should be read from the left-hand scale; those to the right, from the right-hand scale.

Figure 10.- Concluded.

(a) $M_\infty = 3.0$.

Figure 11.- Variation of p/p_∞ with x/d for $M_j = 3.68$. All four nozzles firing.

(b) $M_\infty = 6.0$. Points to the left of the break in the curve should be read from the left-hand scale; those to the right, from the right-hand scale.
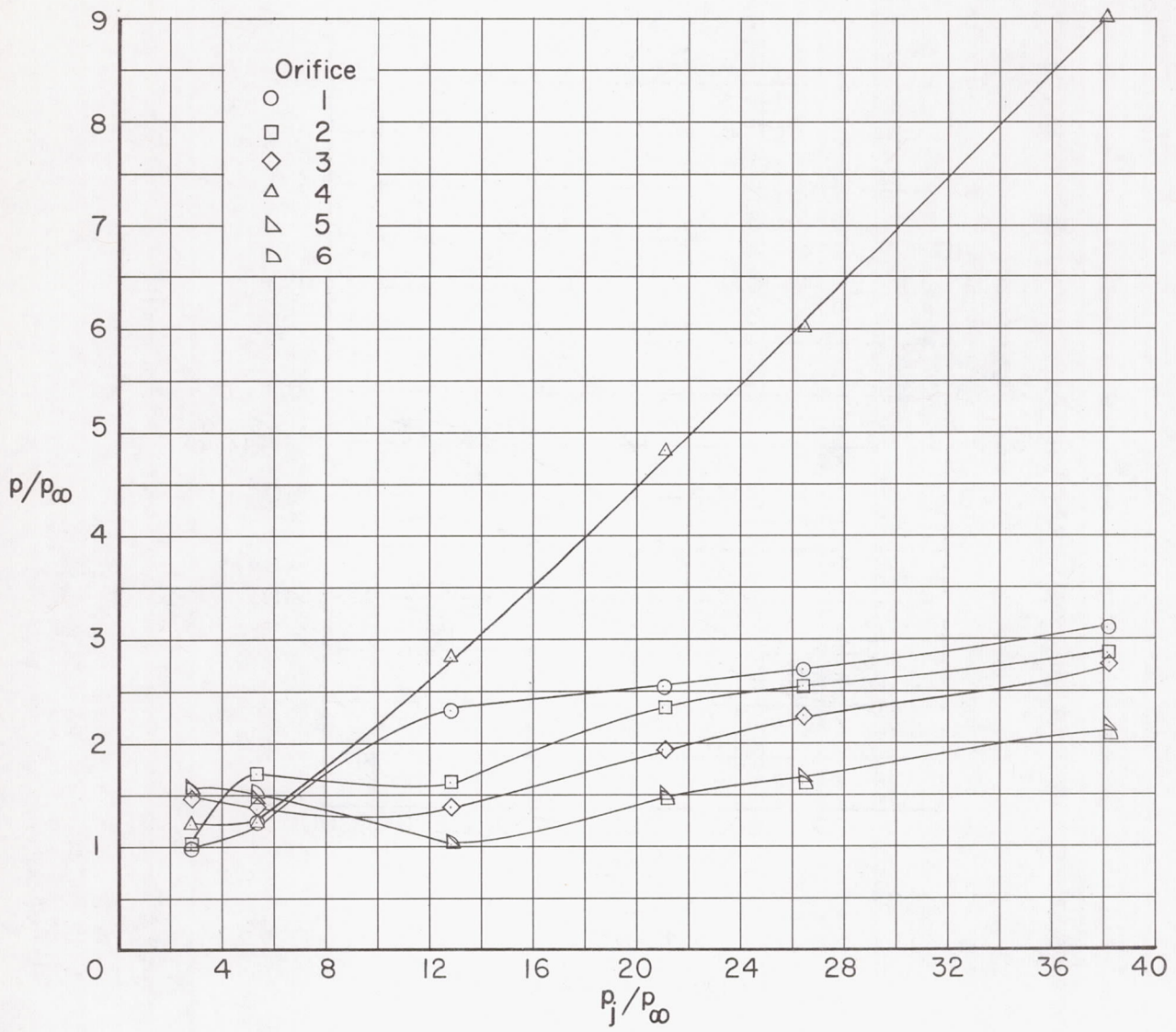
Figure 11.- Concluded.

(a) $M_\infty = 3.0$.

Figure 12.- Variation of p/p_∞ with x/d for $M_j = 3.68$. Nozzle 1 firing.

(b) $M_\infty = 6.0$. Points to the left of the break in the curve should be read from the left-hand scale; those to the right, from the right-hand scale.

Figure 12.- Concluded.

(a) $M_\infty = 3.0$.

Figure 13.- Variation of p/p_∞ with p_j/p_∞ for $M_j = 2.20$. All four nozzles firing; $\alpha = 0^0$.
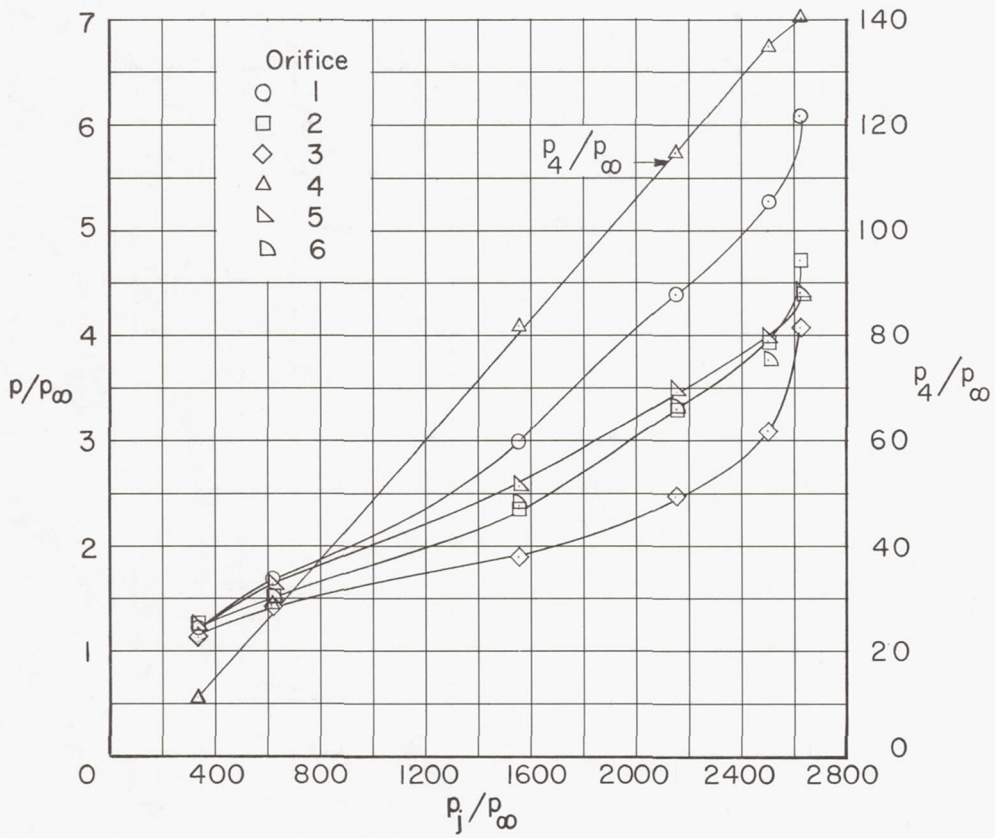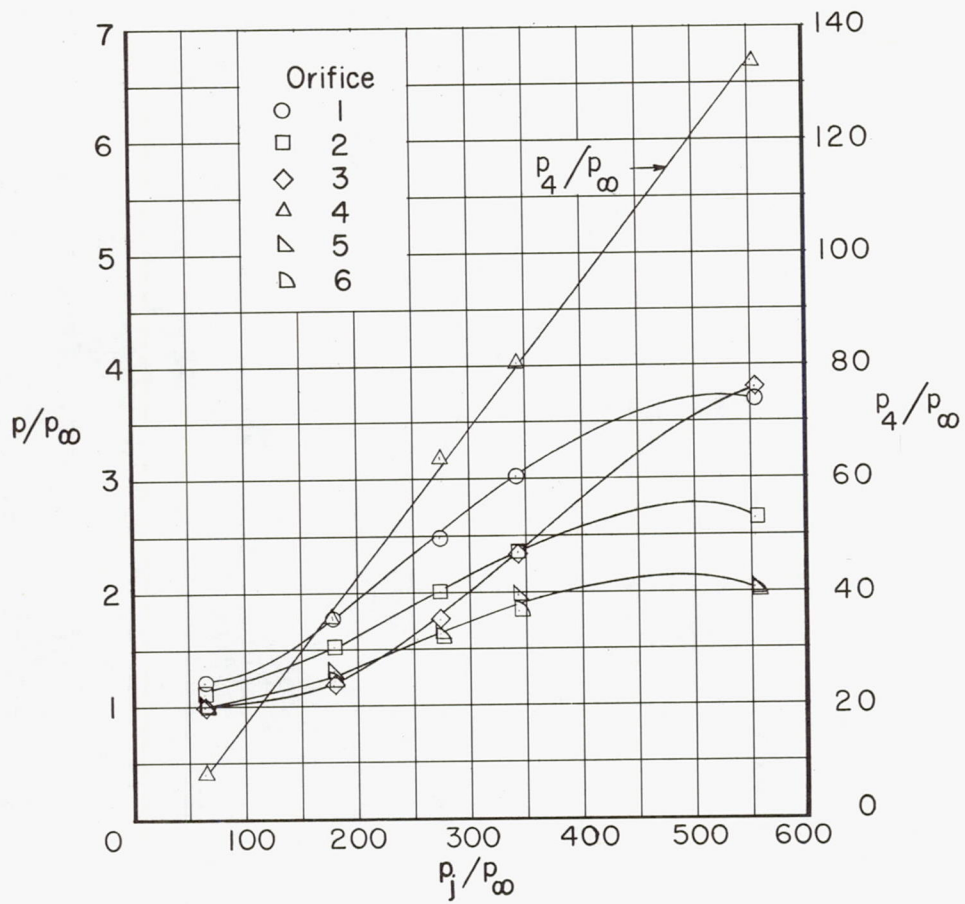
(b) $M_\infty = 6.0$.

Figure 13.- Concluded.

(a) $M_\infty = 3.0$.

Figure 14.- Variation of p/p_∞ with p_j/p_∞ for $M_j = 3.68$. All four nozzles firing; $\alpha = 0^0$.
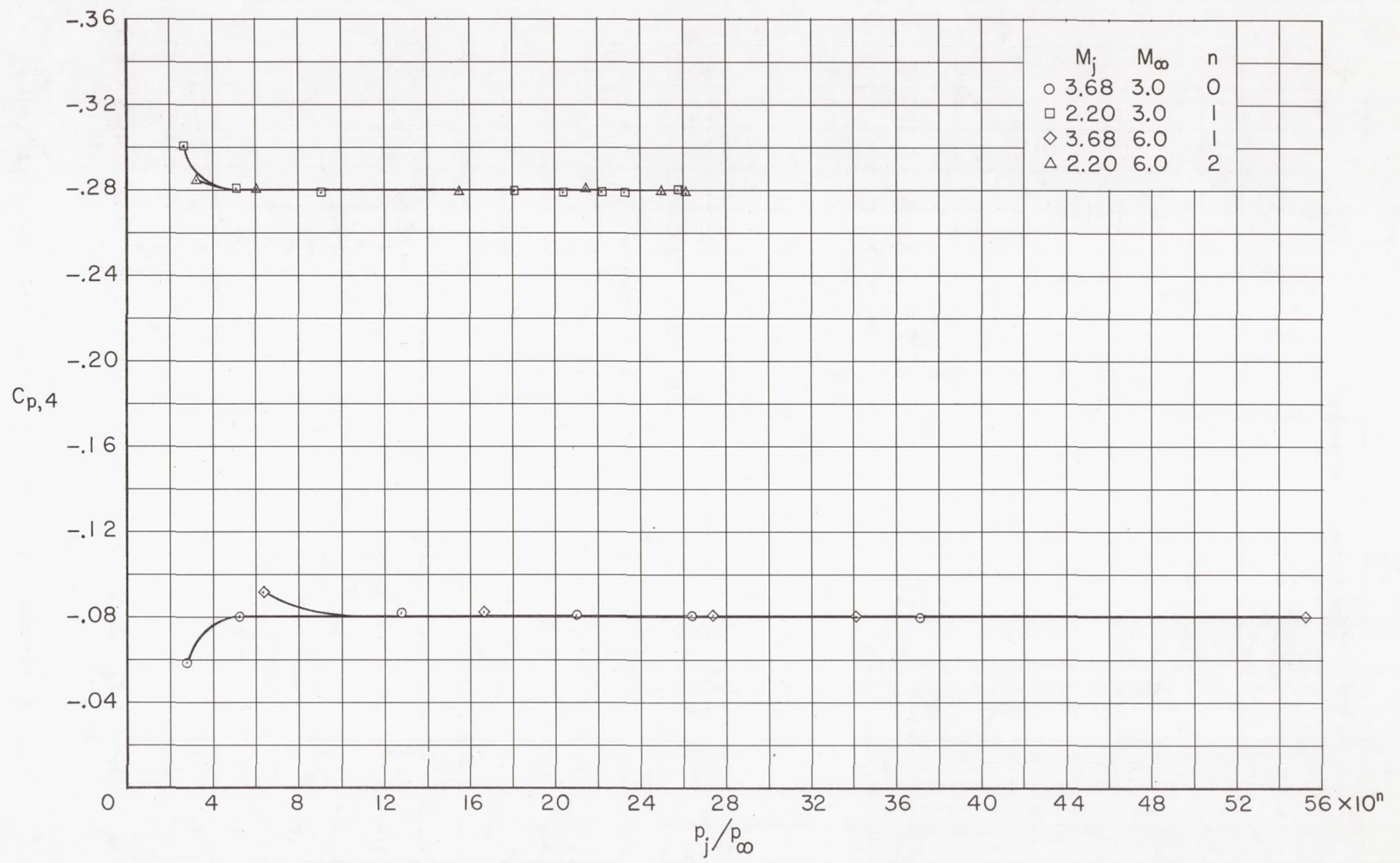
(b) $M_\infty = 6.0$.

Figure 14.- Concluded.

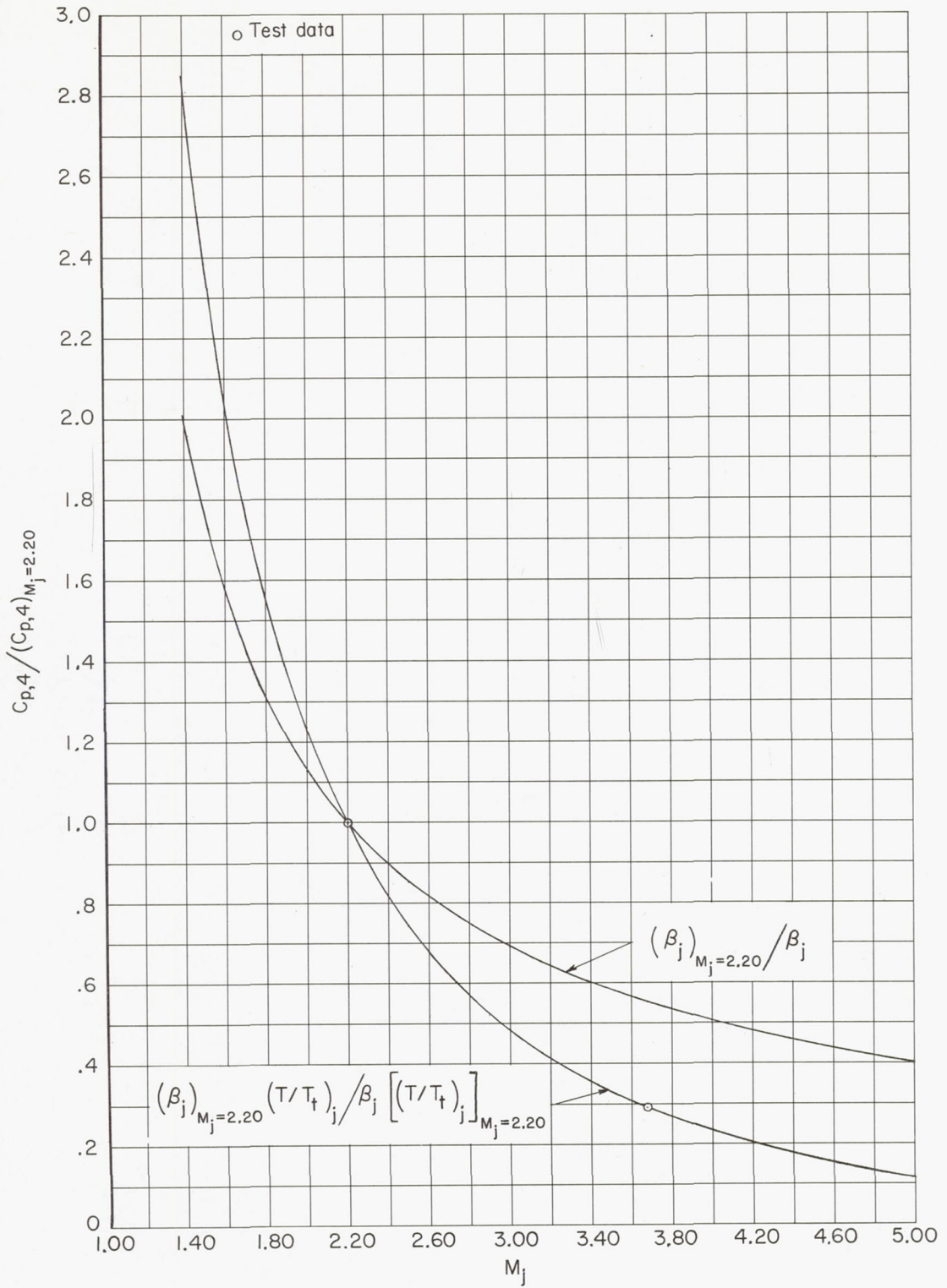Figure 15.- Variation of $C_{p,4}$ with p_j/p_∞

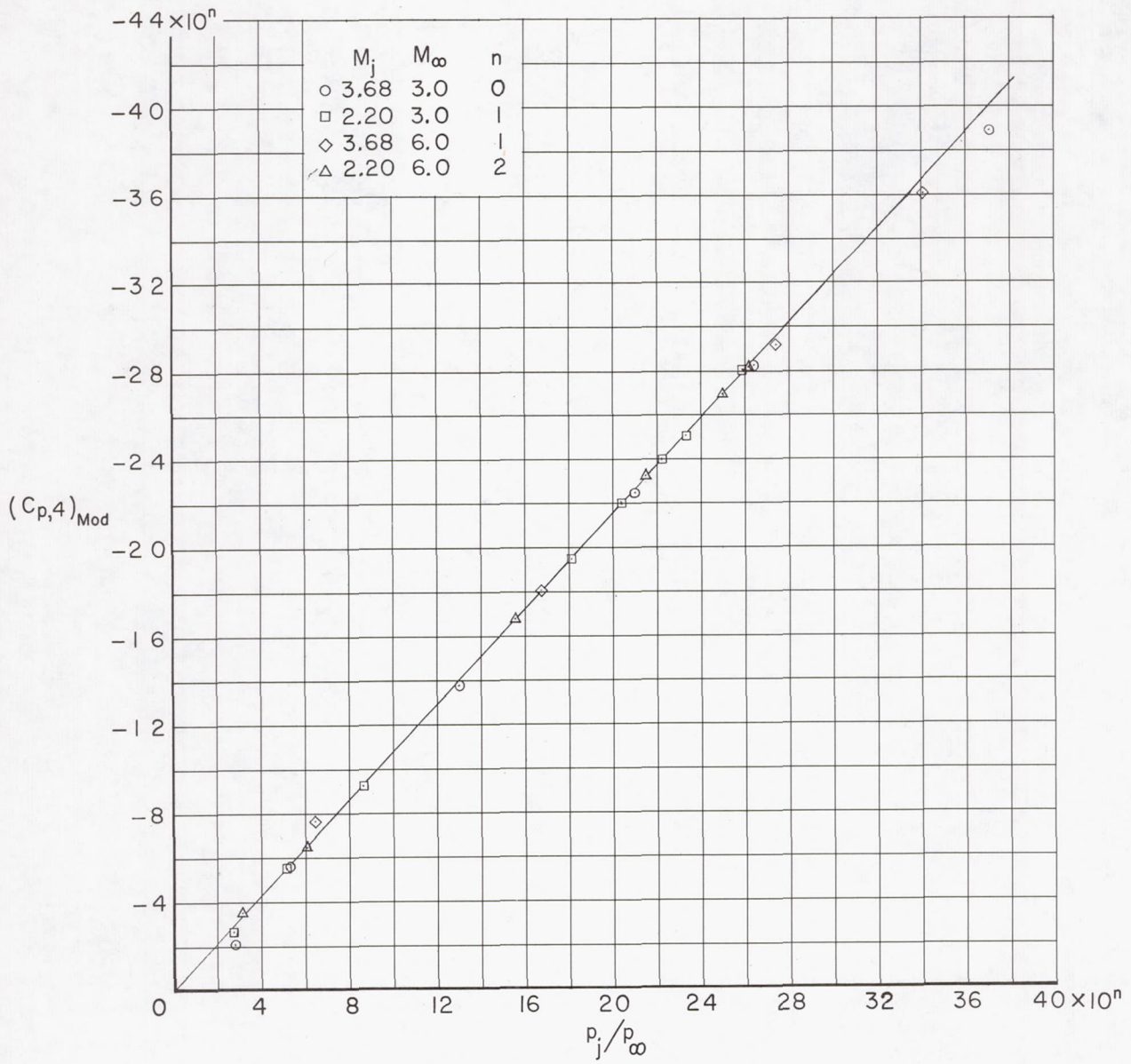Figure 16.- Comparison of data and possible correlating parameters relating $C_{p,4}$ to M_j.

Figure 17.- Variation of modified pressure coefficient with p_j/p_∞.

The chart legend reads:

	M_j	M_∞	n
○	3.68	3.0	0
□	2.20	3.0	1
◇	3.68	6.0	1
△	2.20	6.0	2

Vertical axis: $(C_{p,4})_{Mod}$ from 0 to -44×10^n

Horizontal axis: p_j/p_∞ from 0 to 40×10^n